

Source and receiver deghosting by demigration-based supervised learning

Thomas de Jonge^{1,2} | Vetle Vinje² | Peng Zhao² | Gordon Poole³ | Einar Iversen⁴

¹Department of Earth Science, University of Bergen, Bergen, Norway

²CGG Services Norway AS, Lilleaker, Norway

³CGG Services, R&D Crompton Way, West Sussex, UK

⁴Department of Earth Science, University of Bergen, Bergen, Norway

Correspondence

Thomas de Jonge, Department of Earth Science, University of Bergen, Allégaten 41, Bergen, 5007, Norway.

E-mail: thomas.jonge@uib.no;
thomas.dejonge@cgg.com

Funding information

Research Council of Norway, the University of Bergen and CGG for funding this work through an industrial Ph.D., Grant/Award Number: 305450

Abstract

Deghosting of marine seismic data is an important and challenging step in the seismic processing flow. We describe a novel approach to train a supervised convolutional neural network to perform joint source and receiver deghosting of single-component (hydrophone) data. The training dataset is generated by demigration of stacked depth migrated images into shot gathers with and without ghosts using the actual source and receiver locations from a real survey. To create demigrated data with ghosts, we need an estimate of the depth of the sources and receivers and the reflectivity of the sea surface. In the training process, we systematically perturbed these parameters to create variability in the ghost timing and amplitude and show that this makes the convolutional neural network more robust to variability in source/receiver depth, swells and sea surface reflectivity. We tested the new method on the Marmousi synthetic data and real North Sea field data and show that, in some respects, it performs better than a standard deterministic deghosting method based on least-squares inversion in the τ - p domain. On the synthetic data, we also demonstrate the robustness of the new method to variations in swells and sea-surface reflectivity.

KEYWORDS

data processing, modelling, noise, signal processing, seismics

INTRODUCTION

Ghosts are the result of a reflection of the up-going seismic wavefield at the sea surface on the source and receiver side as shown in Figure 1 (we do not consider the direct wave in this research). A consequence of this ghost reflection is that a reflection from a subsurface structure (black ray in Figure 1a) will be followed by a source ghost, a receiver ghost and a combined source–receiver ghost that elongates and distort the seismic signature. These events interfere constructively and destructively at different frequencies and create a complex recorded trace (Figure 1b). As a result, we observe peaks and notches in the frequency spectrum (Figure 1c). Ghost notches within the seismic bandwidth are problematic because they

attenuate some frequencies and reduce the temporal resolution (Carlson et al., 2007; Poole, 2013). Removing ghosts improves the bandwidth, resolution and signal-to-noise-ratio of the seismic data, bringing benefits for seismic inversion and geological interpretation (Song et al., 2015). Referring to Figure 1a, a successful source and receiver deghosting would imply that up-going energy on the source side (green and blue rays) and down-going energy on the receiver side (red and green rays) will be removed. In other words, we remove the source, receiver and source–receiver ghosts (blue, red and green rays).

The frequency and amplitude of the ghost notches are dependent on the reflectivity and incidence angle at the water surface, the depth of the source and receivers and the water

This is an open access article under the terms of the Creative Commons Attribution License, which permits use, distribution and reproduction in any medium, provided the original work is properly cited.

© 2022 The Authors. *Geophysical Prospecting* published by John Wiley & Sons Ltd on behalf of European Association of Geoscientists & Engineers.

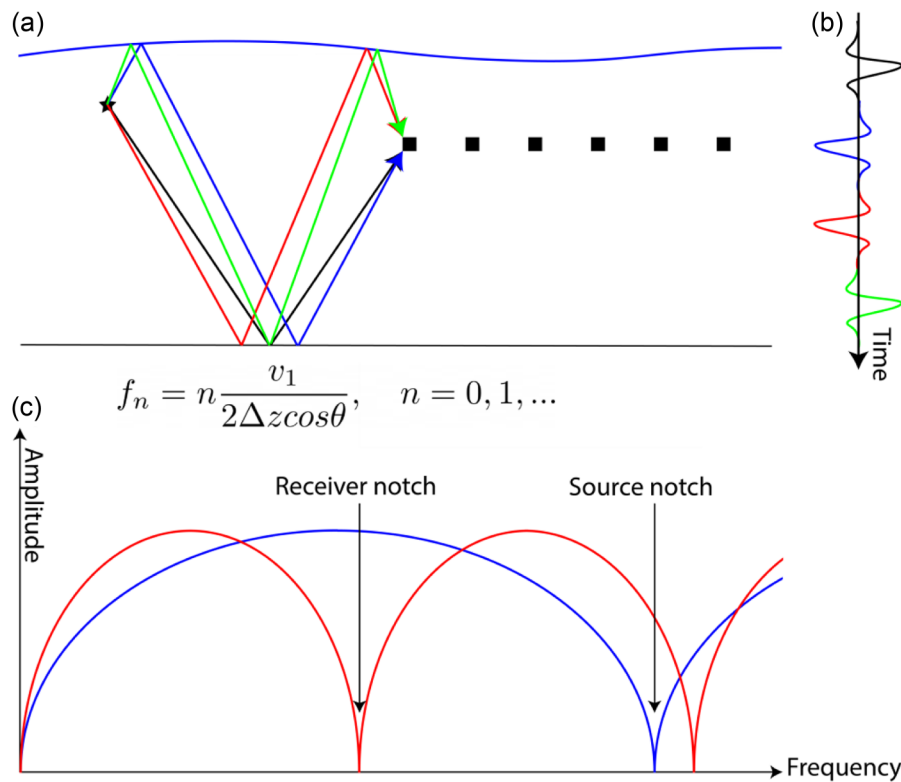


FIGURE 1 (a) Ray paths from a source (star) to receivers (squares) of the primary (black), source ghost (blue), receiver ghost (red) and source–receiver ghost (green). (b) The primary and ghosts in the time domain for one receiver. (c) Ghost functions for the source (blue) and receiver (red). The ghost notch frequency formula (Aytun, 1999) is shown in Figure 1c, where v_1 , Δz , and θ are the water velocity, source/receiver depth, and incidence angle, respectively.

velocity. With an increase in source or receiver depth, there is a decrease in the notch frequency as shown in Figure 1c and the following equation (Aytun, 1999):

$$f_n = n \frac{v_1}{2 \Delta z \cos(\theta)}, \quad n = 0, 1, \dots, \quad (1)$$

where v_1 , Δz and θ are the water velocity, source/receiver depth and incidence angle, respectively. The ghost notch at 0 Hz follows this rule when $n = 0$ and is present regardless of the source and receiver depth. Removing the 0 Hz notch will recover valuable low-frequency information.

Historically, the conventional seismic acquisition solution to the deghosting problem was to locate sources and receivers at relatively shallow depths, typically 5–9 m and to limit the processing and imaging to the frequencies below the first notch. The deghosting was done by deterministic deconvolution (Jovanovich et al., 1983) with the assumption of vertical ray paths and a best-guess sea surface reflectivity. Although other approaches, such as slant streamers (Bearnth & Moore, 1989) or over-under streamers (Hill et al., 2006), were proposed, shallow sources and receivers dominated until the recent advent of broadband seismic acquisition. First, a multi-component streamer approach was proposed

by Carlson et al. (2007), which allowed the streamers to be towed deeper, enhancing the low frequencies. Later, variable-depth streamer acquisition and processing solutions were also proposed (Soubaras & Dowle, 2010; Soubaras et al., 2012; Rickett et al., 2014).

These new configurations in acquisition help to attenuate the receiver side ghost and illustrate the benefits of broadband seismic. However, changes in acquisition geometry alone cannot solve the deghosting problem. For multi-sensor acquisition, the particle velocity measurements are typically noisy and unusable for frequencies below 15–20 Hz (Peng et al., 2014; Mellier & Tellier, 2018; Poole & Cooper, 2018). For variable-depth acquisition, notch diversity dilutes the impact of the receiver ghost over a range of frequencies, but a processing solution is still necessary to remove the receiver ghost wavefield. In addition, both acquisition methods suppress only the receiver side ghost, leaving the source side ghost untouched.

Consequently, source and receiver side deghosting of single-sensor (hydrophone) seismic data is still important. The simplest single-sensor deghosting method consists of deterministic deconvolution as mentioned above. In the past decades, more advanced methods have been introduced. Aytun (1999) modelled a flat streamer receiver ghost and

removed the ghost in the fourier-wavenumber (f - k) domain. Soubaras (2010) used joint deconvolution of migration and a mirror migration. Amundsen et al. (2013b, 2013a) perform a space-domain deghosting based on a Green's function. Amundsen and Zhou (2013) presented a source and receiver deghosting method using the inverse Fourier transform. Furthermore, frequency-slowness domain inversion for deghosting was described by Zhang et al. (2018). In addition, Poole (2013) and King and Poole (2015) performed a τ - p domain inversion for deghosting.

Recently, multiple papers using neural networks in seismic processing have been published. Examples of seismic processing applications of a network are interpolation (Greiner et al., 2019; Fang et al., 2021), denoising (Klochikhina et al., 2020), seismic interference noise attenuation (Sun et al., 2019) and debubbling (de Jonge et al., 2021). An advantage of a neural network is its ability to recognize patterns in the data and adapt to changing patterns. An example of this is given by de Jonge et al. (2021), who showed how a generalized network can debubble data when the source signature changes from shot to shot.

We have found three papers using machine learning for the application of deghosting. Vrolijk and Blacquiere (2020) use a neural network for source deghosting in the common receiver domain. They use conventional receiver deghosting in the common shot domain to create training data and later apply a trained network in the common receiver domain for source deghosting. A drawback with this approach is that the quality of the conventional receiver deghosting used in the training could limit its accuracy. Almuteri and Sava (2021) use a network for deghosting trained on the Marmousi model and Sigsbee model and tested on the Amoco statics test model. Their method needed the real data acquisition geometry and seafloor bathymetry to create training data. Peng et al. (2021) demonstrated a new network structure called DUNet on a deghosting example. However, they use conventional deghosting on part of the survey to create training data with and 'without' ghosts and apply the trained network to the rest of the survey.

A challenge with supervised neural networks is acquiring training data that contain complex features similar to the real data. Some papers show how to use pure synthetic data to train a network that is later used on real data (Zu et al., 2020; Qu et al., 2021). Other papers show how to train a network on synthetic data and use real data for fine-tuning (Cunha et al., 2020; Li et al., 2020). Another option is to use conventional deghosting methods to create training data (Peng et al., 2021). In addition, some papers utilize similarities between training and inference datasets in two different domains, respectively (Siahkoochi et al., 2018; Greiner et al., 2019; Vrolijk & Blacquiere, 2021).

In this paper, we propose a new approach for source and receiver deghosting using demigration-based supervised

learning for hydrophone-only seismic data. We use the acronym DEGDEM (DEGghosting using DEMigration-based supervised learning) for this method. Training data are modelled by Kirchhoff demigration (Santos et al., 2000a) from a pre-stack depth migration (PSDM) image creating a set of ghosted and non-ghosted shot gathers with the real source/receiver geometry for the training. The demigrated shot gathers are termed the *synthesized data* (as opposed to synthetic data) as they are generated from PSDM images from real recorded data. There are several advantages of DEGDEM. First, we do not need to build a detailed P-wave velocity and density model for the synthetic modelling. Instead, a smooth velocity model is used, which is also used in the migration and is easily available. Second, for a given velocity model, the inverse of true-amplitude migration is true-amplitude demigration (Santos et al., 2000b) so the training data will be similar to the real data.

The proposed method is used on real data from the North Sea, Tampen area (CGG, 2020). In addition, we tested DEGDEM on synthetic finite-difference data using the Marmousi model (Martin et al., 2006). The tests on the Marmousi model allowed us to quantify the effect of training approaches to make the network adaptable to changes in receiver depth and the reflection of the sea surface. It also allowed us to quantify the sensitivity to residual ghosts in the PSDM image. We also test DEGDEM on multiples with ghosts. This test is important because the training data from the demigration does not contain multiples. Results on both synthetic and real data are compared with a conventional deghosting method by Poole (2013).

METHODOLOGY

Training, validation and test data

A challenge with supervised neural networks is to find or create training data – with and without ghosts – that is similar to the real data. Ideally, using real data as training data would be the preferred option. However, obtaining marine seismic data without ghosts is not straightforward. One option is to use an existing hydrophone-only deghosting method to attenuate the ghost and use data before and after deghosting for training (Peng et al., 2021). The main problem with this approach is that the network is trained on data that are not perfectly deghosted. For that reason, it is hard for the network to achieve better results than conventional deghosting. A second option is to use deghosting from multi-sensor streamer acquisitions. This would involve training a network to produce the sum of pressure and vertical velocity data from hydrophone data and using this network for a nearby hydrophone-only dataset. Towed streamer accelerometer data are not always available, and the accelerometer recordings

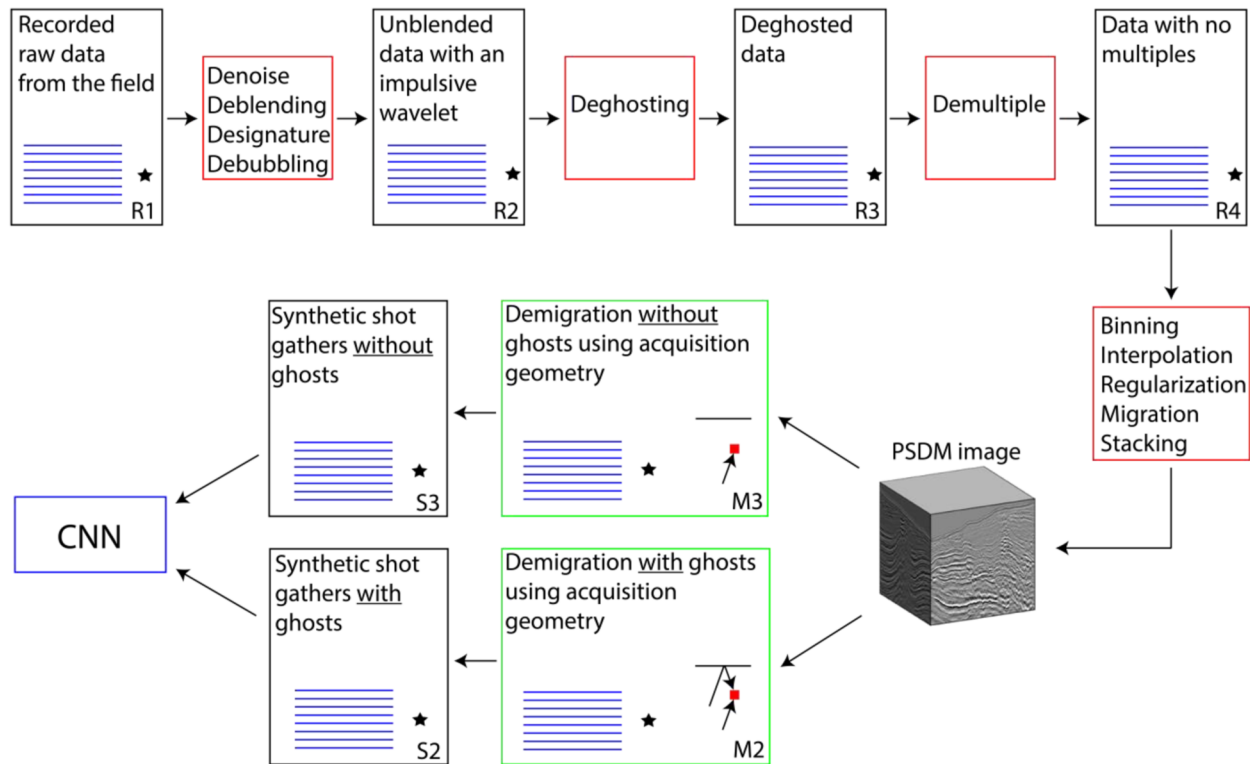


FIGURE 2 An illustration of the DEGDEM workflow used in this paper. Several processing steps remove unwanted energy and are followed by migration to obtain a stacked PSDM image followed by demigration to generate synthesized shot gathers for the training.

are often noisy, particularly at low frequencies. Another option is to use synthetic data generated in a velocity–density model using, for example, finite-difference modelling. The challenge with this approach is building a velocity–density model, which will lead to finite-difference data mimicking the spectral content, phase shift and event complexity of the real data.

The new approach, DEGDEM (DEGhosting using DEMigration-based supervised learning), described in this paper involves generating *synthesized* shot gathers by Kirchhoff demigration (Hubral et al., 1996; Santos et al., 2000a) from a seismic image. The seismic image is a representation of the true subsurface reflectivity and is created from seismic data using Kirchhoff migration. As Kirchhoff migration and demigration can be regarded as inverse processes (Hubral et al., 1996; Santos et al., 2000b) or adjoint processes (Schuster, 1993), the synthesized seismic data will closely resemble the recorded seismic data. The demigration approach is described in more detail in the subsection ‘Kirchhoff demigration’.

The DEGDEM workflow is illustrated in Figure 2. As part of a standard processing flow, recorded data proceed through several processing steps including denoise, deblending, designature, debubbling, deghosting and demultiple. This creates shot gathers with (ideally) an impulsive wavelet, no ghosts and no multiples in Figure 2-R4. These data are then binned, interpolated and regularized into a number of offset

classes, which are Kirchhoff migrated and finally stacked to create the pre-stack depth migration (PSDM) image. Using the migration velocity, this PSDM image is demigrated to create synthesized shot gathers with ghosts (Figure 2-S2) and without ghosts (Figure 2-S3) using the real source and receiver positions in the training area. A number of shot gather pairs (S2–S3) are used in the training process. We use the terminology *training area* for the area in the PSDM image that is used to create synthesized data, later used as training data. The *prediction area* is where we apply the network. We can use identical training and prediction areas or use a subset of the prediction area as the training area. Moreover, the network can either be used on the data from the same acquisition (step R2 in Figure 2) or another acquisition.

Kirchhoff demigration

Santos et al. (2000a) show how to use Kirchhoff demigration to compute what we term *synthesized seismograms*. True-amplitude Kirchhoff demigration can be regarded as the inverse process (Hubral et al., 1996; Santos et al., 2000b) or adjoint process (Schuster, 1993) of true-amplitude Kirchhoff migration, where it is described as seismic modelling with the Kirchhoff integral. It involves returning

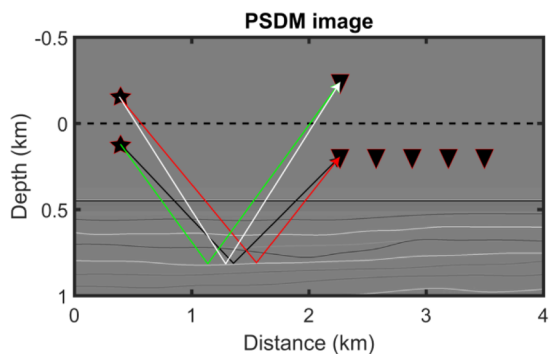


FIGURE 3 An illustration showing how to create data with ghosts using Kirchhoff demigration from a PSDM image. The source and receivers are placed above the sea surface (dotted black line) to create the ghosts. Water velocity is used above the sea surface.

from a true-amplitude depth migrated section to the original pre-migration common offset data in time. Demigration has particularly suited for machine-learning-based training because the synthesized data are similar to the original data going into the migration. We use a PSDM-stacked image, a smooth velocity model and Kirchhoff demigration to create synthesized training data. With Kirchhoff demigration, we can create synthesized data for any acquisition geometry. We create the source, receiver and source–receiver ghosts by placing the source and receiver in a mirror position above the sea surface as illustrated in Figure 3. Later, we multiply by the sea surface reflectivity to get the correct polarity and amplitude. A ghosted shot gather, $D_i(x_j, t_k)$, is modelled by a linear combination of four ghost-free shot gathers ($P_i(x_j, t_k)$, $P_i^{SG}(x_j, t_k)$, $P_i^{RG}(x_j, t_k)$, $P_i^{SRG}(x_j, t_k)$):

$$D_i(x_j, t_k) = P_i(x_j, t_k) + RP_i^{SG}(x_j, t_k) + RP_i^{RG}(x_j, t_k) + R^2P_i^{SRG}(x_j, t_k), \quad (2)$$

where P is the dataset using the actual source and receiver locations, P^{SG} is the dataset using the mirror source location, P^{RG} is the dataset using the mirror receiver location, P^{SRG} is the dataset using the source and receiver mirror locations, R is the reflectivity of the water surface, i is the shot number, x_j is the offset and t_k is the time. This means that we create four datasets: (1) the ghost-free primary, P , by using the original source and receiver positions (black ray in Figure 3), (2) the source ghost, P^{SG} , by placing a source at the mirror position above the sea surface (red ray in Figure 3), (3) the receiver ghost, P^{RG} , by placing a receiver at the mirror position above the sea surface (green ray in Figure 3) and (4) the source–receiver ghost, P^{SRG} by placing both a receiver and a source at the mirror positions above the sea surface (white ray in Figure 3). The reflectivity of the water surface, R , results in a polarity shift when multiplied with arrivals (2)

and (3). The ghost-free dataset is P , while the dataset with ghosts is created using Equation (2), which is a linear combination of all four datasets. As a result, we get synthesized data with and without ghosts as shown in Figure 4b,c. During the training, the input to the network is synthesized shot gathers with ghosts (Figure 5a), and the outputs are synthesized shot gathers without ghosts (Figure 5b).

Convolutional neural networks

A convolutional neural network (CNN) uses convolutions instead of general matrix multiplications (Goodfellow et al., 2016). By doing this, the network has sparse interactions between the neurons in the network. In particular, the kernel size determines the number of interactions from one layer to the next. A CNN is typically used when it is assumed that the meaningful features are local. As a result, sparse interactions can save memory and computational cost.

In this paper, we used a CNN structure called a U-net (Ronneberger et al., 2015). This structure is made up of an encoder and decoder with skip connections. The encoder downsamples the number of pixels, and the decoder upsamples the number of pixels. Various pooling functions (maximum, average, L2, etc.) can be used to downsample the number of pixels. In contrast, a transposed convolution can be used to upsample the number of pixels. Transposed convolution is an operation that goes in the opposite direction of a normal convolution. Dumoulin and Visin (2016) show several examples of transposed convolution. The U-net is different from an encoder–decoder because it contains skip connections that copy feature maps from one layer to another. Since the U-net uses downsampling and consequently reduces the image size, it is also more efficient than a CNN with no downsampling. Another benefit of the U-net downsampling is the increased receptive field of the network (Lucas et al., 2018). In contrast, only the size of the convolutional kernel determines the receptive field of a CNN with no downsampling.

The structure of our U-net has also been used in de Jonge et al. (2021) showing good results. Furthermore, the structure is shown in Figure 6 and the hyperparameters are shown in Table 1. In addition, we compare this U-net with the Dunet presented by Peng et al. (2021). The Dunet has many structural similarities with the U-net. More information about the Dunet can be found in Peng et al. (2021). These two networks are used for all our tests. That said, the goal of this paper is not to find the optimal network structure, rather it is focused on creating training data that can be used to get high-quality deghosted data. We believe that training data are one of the most important aspects when using a neural network to achieve good deghosting results.

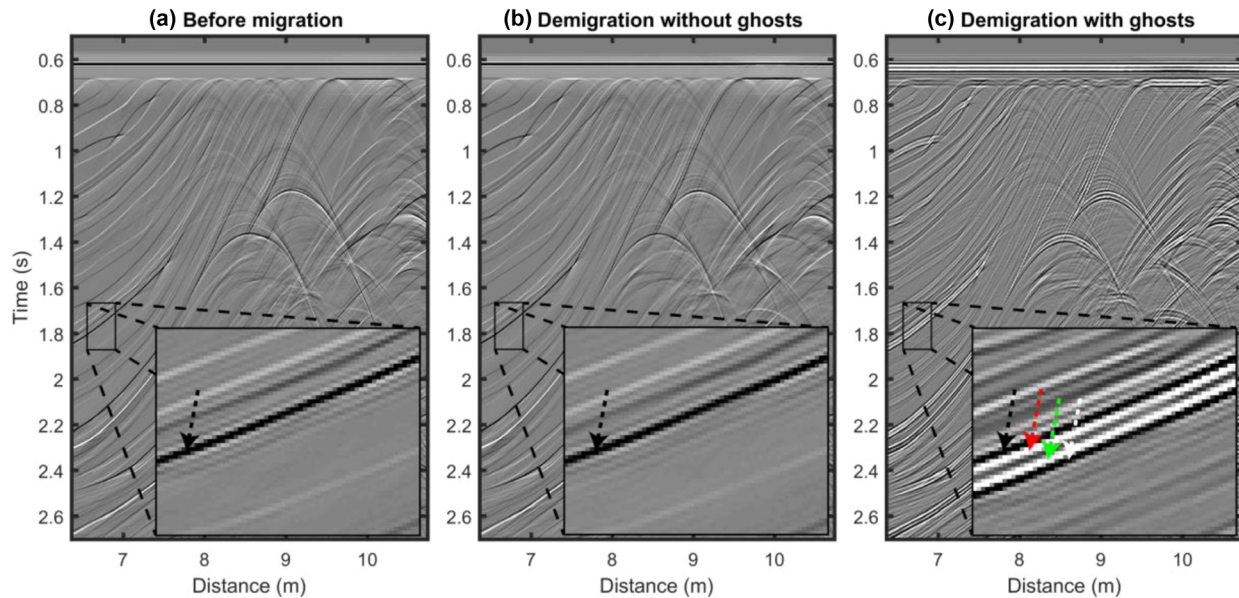


FIGURE 4 Common channel gathers before migration (a), demigration without ghosts (b), and demigration with ghosts (c). Data before migration are modelled with FD. A zoom is used in all three plots focusing on a single event where arrows highlight the primary (black), source ghost (red), receiver ghost (green) and source–receiver ghost (white).

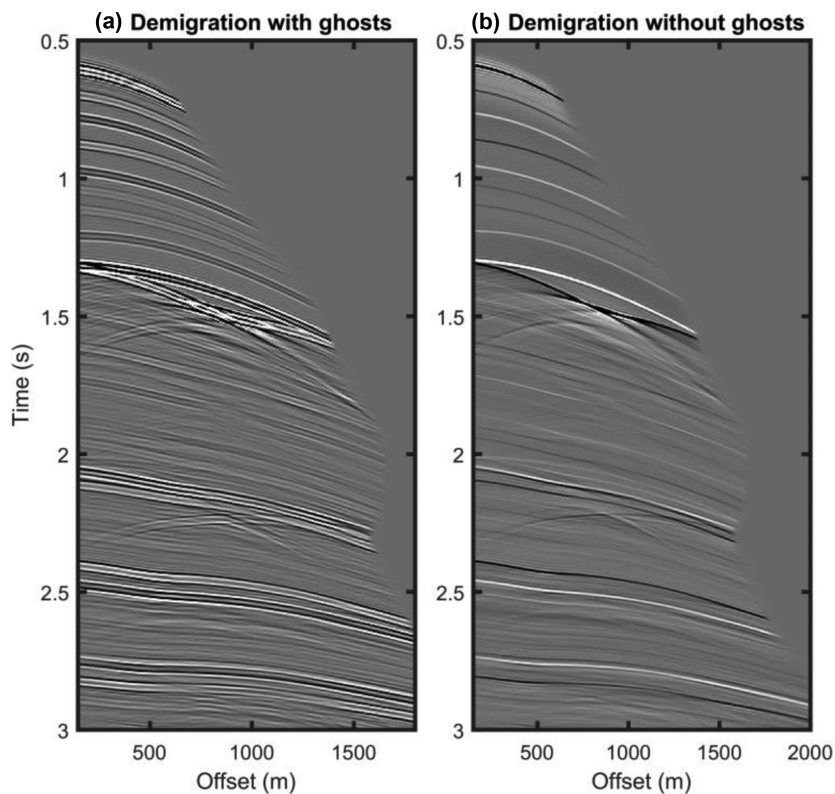


FIGURE 5 Demigrated shot gather with ghosts (a) and without ghosts (b).

RESULTS

This section is divided into two parts: (1) synthetic data, which focuses on various tests to understand the problems and

advantages of DEGDEM (DEGHOSTING using DEMigration-based supervised learning), and (2) real data, which focuses on one specific example from the Tampen area in the North Sea.

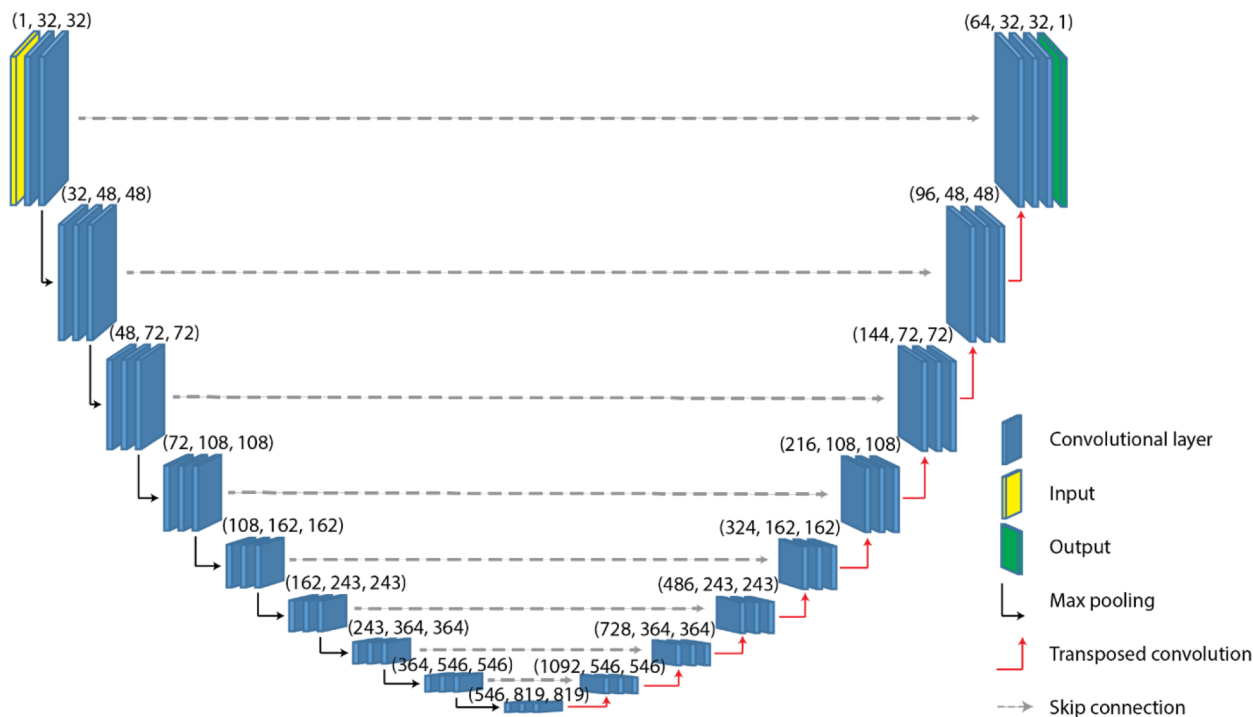


FIGURE 6 The U-net structure used in this paper. The numbers represent the number of feature maps at each stage in the network. The hyperparameters are shown in Table 1.

TABLE 1 Hyperparameters used in the U-net shown in Figure 4

Loss function	Mean square error
Optimization	Adam (learning rate = 0.0001)
Kernel sizes for convolution	3×3
Kernel size for max pooling	2×2
Kernel size for transposed convolution	2×2
Stride for convolution	1×1
Stride for max pooling	2×2
Stride for transposed convolution	2×2
Activation function	ReLU
Batch size	4
Epochs	200

Synthetic data

Evaluating the quality of the deghosting results is often difficult on real data because we do not know the true ghost-free data. For that reason, we have conducted a synthetic analysis. In addition, this synthetic analysis can tell us more about the advantages and limitations of using DEGDEM. In the synthetic analysis, we used the Marmousi model (Martin et al., 2006) and acoustic finite-difference (FD) modelling to model data with and without the ghosts. The DEGDEM workflow for the synthetic analysis is shown in Figure 7 and is similar to the workflow shown in Figure 2. The FD data were modelled using the Marmousi P-wave velocity and density

(Martin et al., 2006) shown in Figure 8. The source is placed at 6 m depth and a streamer with hydrophones at 20 m depth. The receiver and shot increments are 12.5 and 6.25 m, respectively. The offset to the first receiver is 147 m. Mirror locations above the sea surface for the source and receiver were used to model the ghosts as described in the section ‘Methodology – Kirchhoff demigration’. As a result, we have two datasets – one with ghosts and one without.

A smooth velocity model (Figure 9a) was used for the travel time calculations in Kirchhoff demigration. This velocity model was a smooth version of the Marmousi model shown in Figure 8. We Kirchhoff migrated and stacked the FD modelled data without ghosts to generate a pre-stack depth migration (PSDM) image shown in Figure 9b. Both the smooth velocity model and the PSDM image were used to create synthesized data with Kirchhoff demigration. The mirror source and mirror receiver technique described in the ‘Methodology – Kirchhoff demigration’ subsection was used to create data with and without ghosts. As a result, we modelled shot gathers with and without ghosts that were used for training the neural network.

In this subsection, we describe several tests to identify some advantages and disadvantages of DEGDEM. The first test, entitled baseline test (first row in Table 2), relates to a neural network trained and tested on ghosts that were modelled using the correct source locations, receiver locations and sea surface reflection coefficient. The second and third tests, entitled the swell wave test and the reflection coefficient test (second and

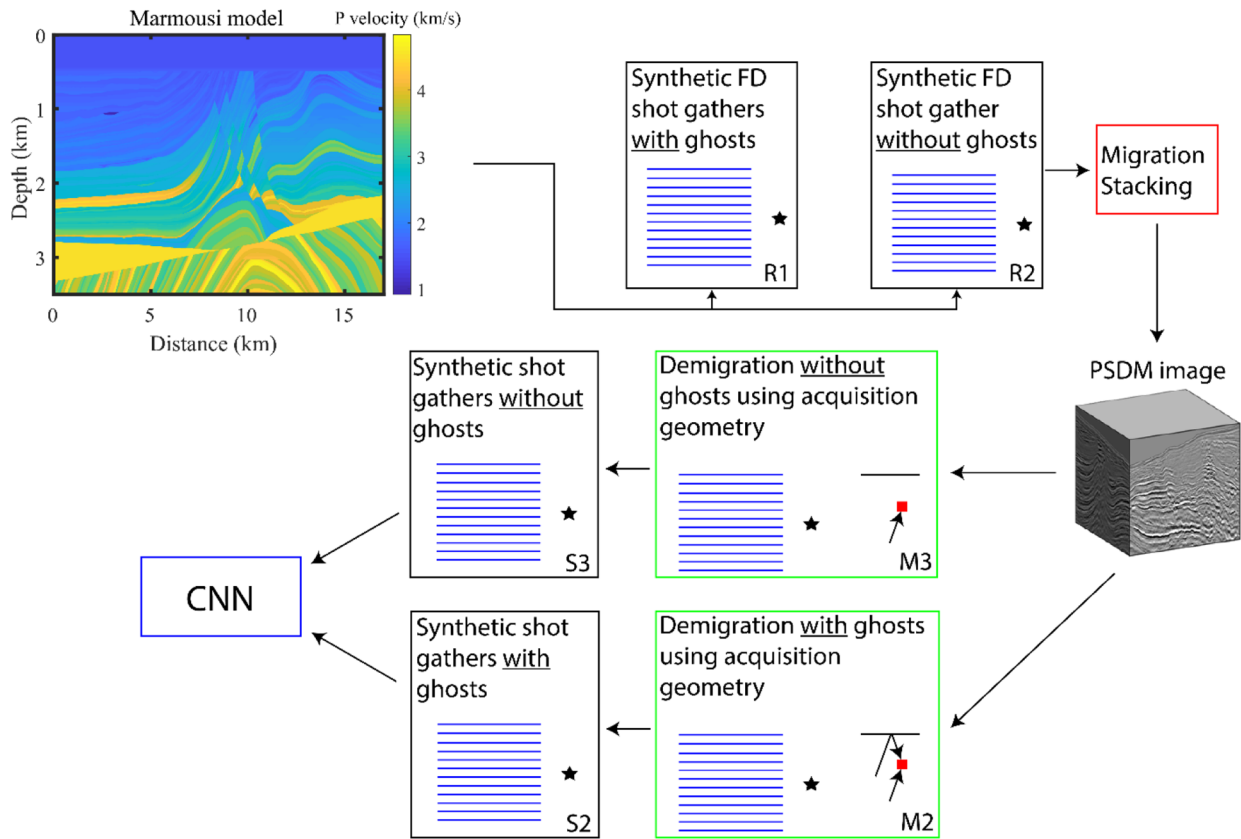


FIGURE 7 An illustration of the DEGDEM workflow used for the synthetic tests. First synthetic data with and without ghosts are modelled using FD and the Marmousi model. The ghost-free data are migrated to obtain the PSDM image. The PSDM image together with Kirchhoff demigration is used to generate synthesized shot gathers with and without ghosts.

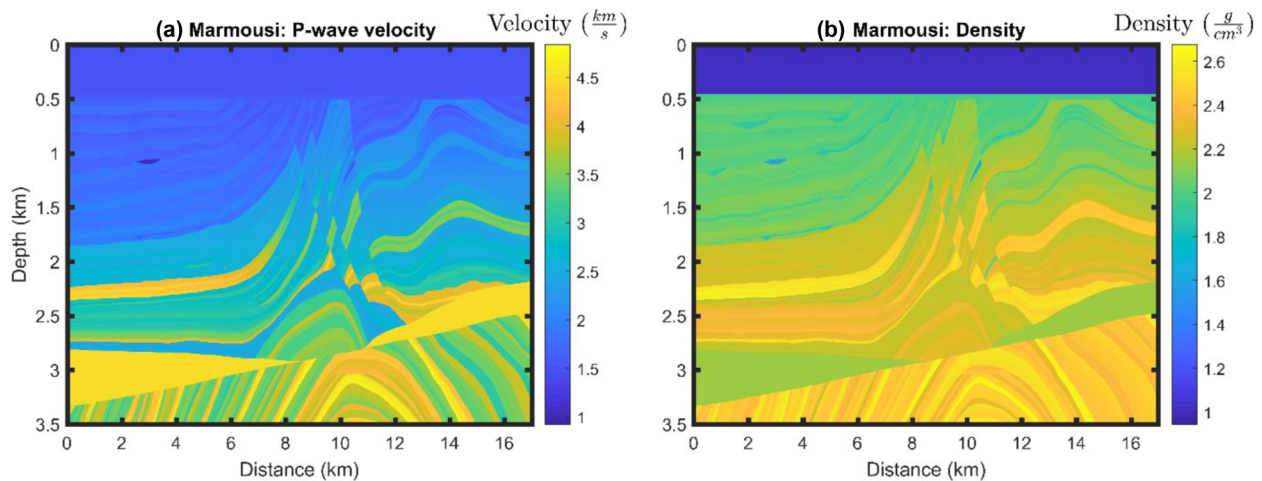


FIGURE 8 The Marmousi models for P-wave velocity (a) and density (b) are used to generate synthetic data.

third rows in Table 2), examine the sensitivity of the network used in the first test to swell waves and changes in the sea surface reflection coefficient. In both the second and third tests, we also re-train the U-net and DUNet using different training data attempting to make the network more robust to swell waves and changes in sea surface reflectivity. The fourth

test, entitled residual ghost (fourth row in Table 2), uses a PSDM image containing residual ghost to generate training data for DEGDEM. This test investigates how sensitive the network is to residual ghost in the PSDM image. The fifth test, entitled multiple test (fifth row in Table 2), investigates if the network can attenuate ghosts of surface-related

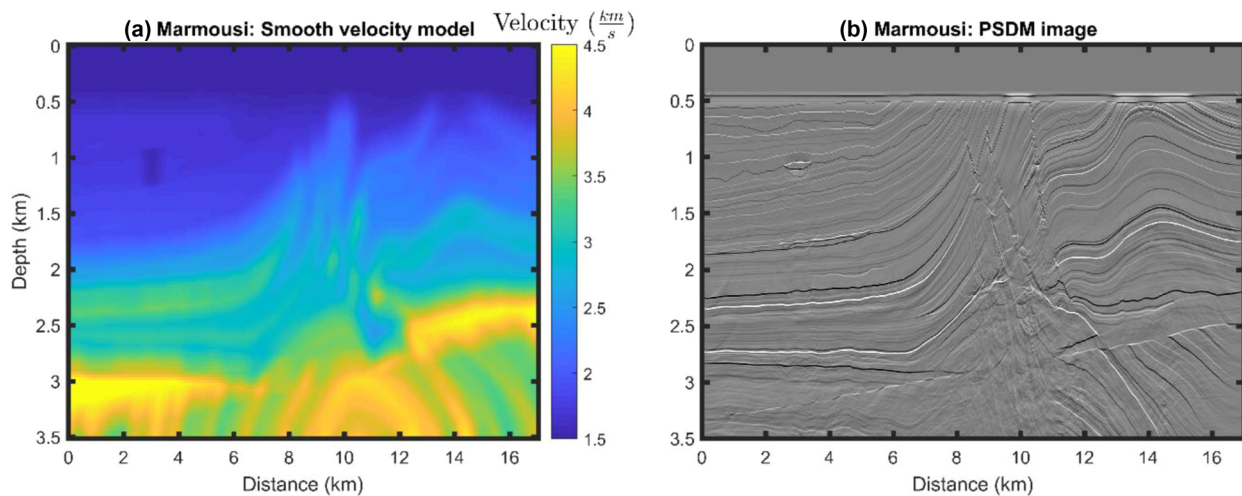


FIGURE 9 Smooth P-wave velocity model (a) and PSDM image (b). Both of these models are used to create synthesized data with Kirchhoff demigration.

TABLE 2 NRMS error (common channel domain, channel 15) when using conventional deghosting, standard DEGDEM (U-net or DUnet) for deghosting, or generalized DEGDEM (U-net or DUnet) for deghosting. Each result is separated into the various tests in this subsection

	Conventional	Standard DEGDEM (U-net)	Standard DEGDEM (DUnet)	Generalized DEGDEM (U-net)	Generalized DEGDEM (DUnet)
Baseline test	0.0030	0.0032	0.0033	N.A.	N.A.
Swell wave test	0.0171	0.0044	0.0064	0.0039	0.0078
Reflection coefficient test	0.0058	0.0039	0.0050	0.0031	0.0028
Residual ghost	0.0171	0.0070	0.0081	N.A.	N.A.
Multiple test	0.0040	0.0042	0.0040	N.A.	N.A.

multiples. This test is important because the synthesized data do not contain surface multiples, in contrast to real data. A summary of all results from this subsection is shown in Figure 10 and Table 2, while more detailed descriptions of the tests are given in their respective subsections. Here, a generalized DEGDEM represents a network that has been trained to be more robust to swell waves or changes in sea surface reflection coefficient.

To quality control our results, we use common channel gathers (channel 15) before deghosting, after deghosting, and the difference. We evaluate a normalized root mean square (NRMS) error measurement in the common channel domain given by the equation:

$$e^{\text{NRMS}} = \frac{e^{\text{RMS}}}{y_{\max} - y_{\min}} = \frac{1}{y_{\max} - y_{\min}} \sqrt{\frac{\sum_{i=1}^n (\hat{y}_i - y_i)^2}{n}}, \quad (3)$$

where y_i is the data without ghosts, \hat{y}_i is the deghosted data and n is the number of samples.

Baseline test

In this test, we trained a network using the DEGDEM workflow shown in Figure 7 using the correct source locations, receiver locations and sea surface reflection coefficient. We used 2340 pairs of synthesized training shot gathers (with and without ghosts) to train the CNN. Afterwards, we applied the CNN on 2340 of FD shot gathers (with ghosts) within the training area and 321 FD shot gathers outside the training area. In the next subsections, all synthetic tests use the same training area and prediction area as in the baseline test. We ran 200 epochs in this test and ensuing tests. We compared the neural network result with the conventional deghosting method of Poole (2013). Figure 11 shows the results using conventional deghosting and DEGDEM (U-net) deghosting within the training area. DEGDEM (U-net), DEGDEM (DUnet) and conventional deghosting NRMS errors were 0.0032, 0.0033 and 0.0030, respectively. The NRMS error was calculated using all samples from 0.5–3 s and 2002–16,607 m. All synthetic tests in the following subsections use the same window

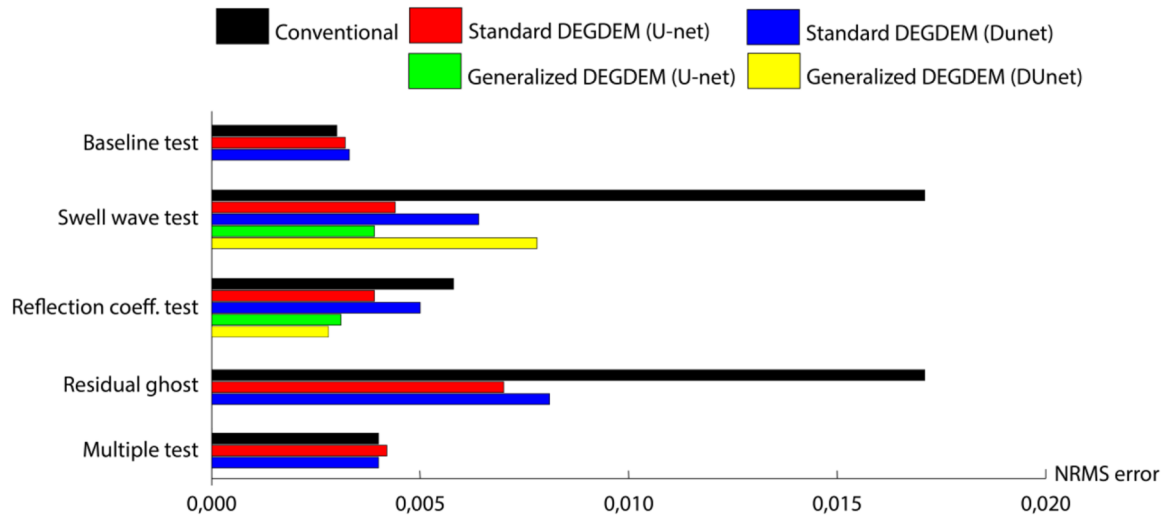


FIGURE 10 Bar graph showing NRMS error (common channel domain, channel 15) when using conventional deghosting, a standard DEGDEM (U-net or DUnet) for deghosting or a generalized DEGDEM (U-net or DUnet) for deghosting. Each result is separated into the various tests in this subsection.

to calculate the NRMS error. The amplitude spectrum in this test and all ensuing synthetic tests were calculated using the same window as the NRMS error. Figure 11 and the NRMS errors demonstrate that DEGDEM and conventional deghosting both have low error. Referring to the amplitude spectra, in general the conventional deghosting worked better than DEGDEM at the ghost peak frequencies, and DEGDEM performed better at the ghost notches (except for the last notch at approximately 75 Hz). DEGDEM may have performed better than conventional deghosting in the ghost notches because the training data were similar to the prediction data, which is one of the advantages when using demigration to create training data. In other words, it was already familiar with the ‘spiky’ nature of the prediction input. The conventional deghosting, on the other hand, was more general and did not have a bias towards any wavelet or geology. We also observe that DEGDEM performed less well in the area of conflicting dips in the centre of the section compared to the DEGDEM in areas of less complex geology. In this perfect scenario, the conventional method performed better than DEGDEM in general. DEGDEM (U-net) was used on FD data outside the training area to demonstrate that the network works on data with similar geology. The results are shown in Figure 12, where the training area is to the right of the dashed line. The NRMS error is shown for each shot and does not change significantly when DEGDEM is applied to data outside the training area. As an additional test, we exclude the central part of the Marmousi model as training data (shown in Figure 13). Data outside the dashed lines were used as training data. The central part of the model contained more complex geology with steeply dipping layers and faults. The amount of training data was still 2340 shot gather pairs by including the test data from the previous test (shown in Figure 12). The results are shown in Figure 13,

where the NRMS error does not change significantly in the central part of the model.

Sensitivity and generalization of streamer depth and sea surface reflection coefficient

Ocean waves, bad weather and the imperfect positioning of receivers are a natural part of a marine seismic acquisition. The sea surface reflection coefficient may also change from shot to shot or with offset and is not always known. Consequently, a ghost model based on nominal reflectivity coefficients and receiver depths may be inaccurate. We will investigate how robust the neural network is to these changes. A key feature of neural networks is their adaptability. Consequently, it may be possible to train a neural network on many different streamer depths and sea surface reflection coefficients. By using this approach, it could be possible to generalize the network. A generalized network would be a big advantage and easy to use on real data. We use the network from the ‘Baseline test’ subsection and train new networks that have been generalized on either streamer depth or sea surface reflection coefficient.

We start by focusing on streamer depth. In our test, we simulated a swell wave that changes the height of the water column above the receivers as shown in Figure 14. For simplification, we model the swell wave as a sinusoid wave:

$$A(x) = B \sin(k(x - \phi)), \quad (4)$$

where B is the amplitude, k is the wavenumber, x is the offset and ϕ is the phase shift. The swell wave parameters are

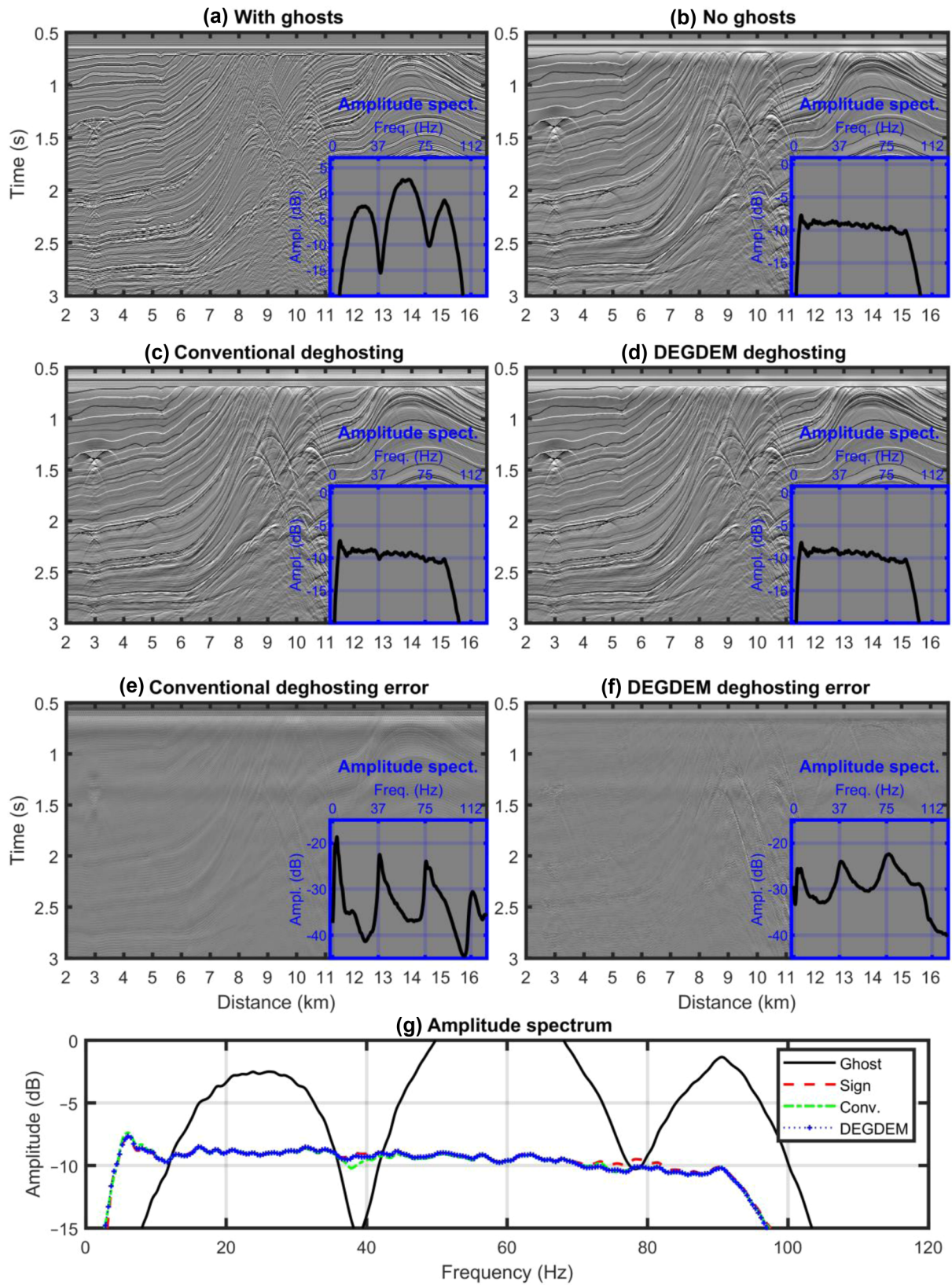


FIGURE 11 Common channel gather (channel 15) displays for (a) data with ghosts; (b) data without ghosts; (c) conventional deghosting; (d) DEGDEM deghosting; (e) residual noise left after conventional deghosting (difference between no ghosts and conventional deghosting); (f) residual noise left after DEGDEM deghosting; (g) amplitude spectrum of data with ghosts (black solid line), without ghosts (red dashed line), conventional deghosting (green dashed line) and DEGDEM deghosting (blue dashed line).

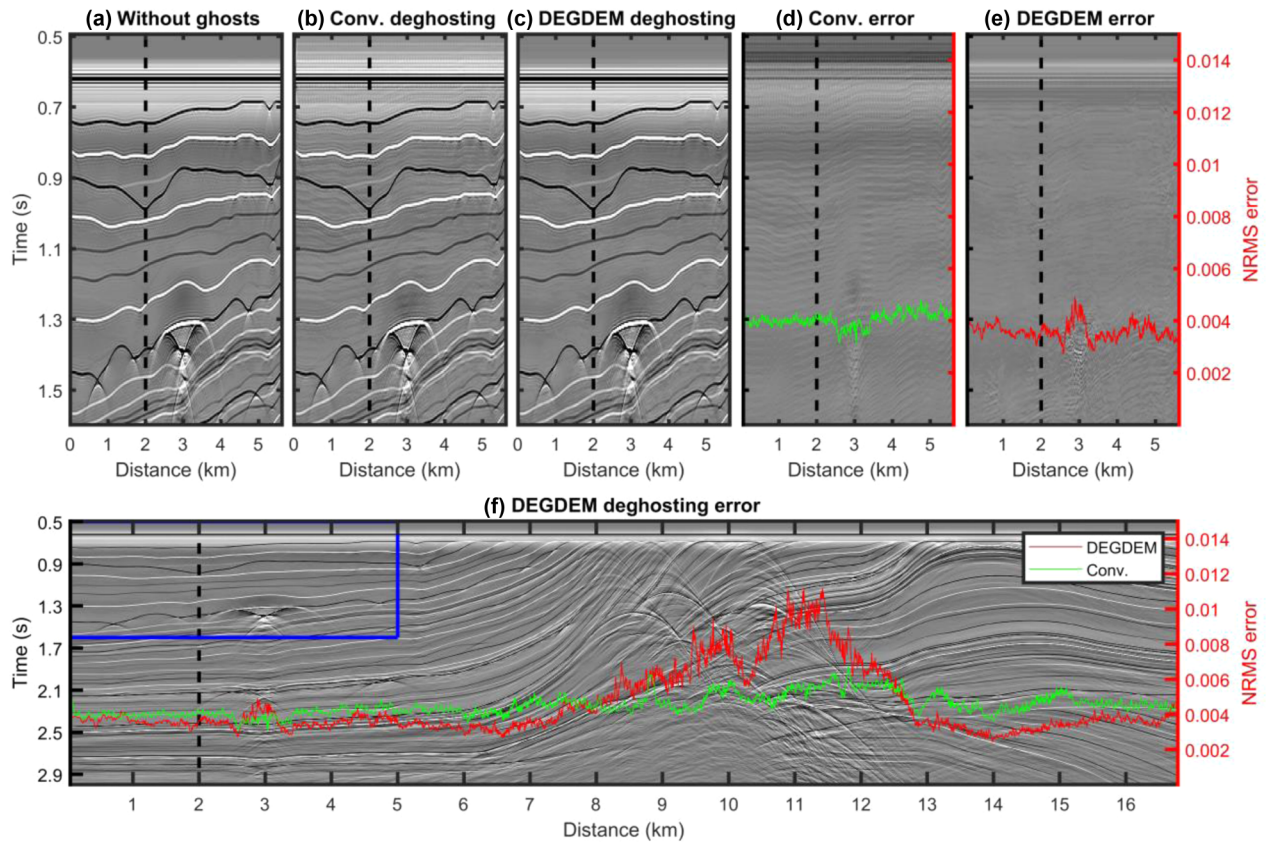


FIGURE 12 Common channel gathers (receiver 15) before deghosting (a), conventional deghosting (g), DEGDDEM deghosting (c), conventional deghosting error (d), DEGDDEM deghosting error (e) and a zoom of the DEGDDEM deghosting (f). The area shown in subfigures a, b, c, d and e is indicated by a blue rectangle in subfigure f. Right of the dashed line is used as a training area. The red and green lines show the NRMS error using DEGDDEM and conventional deghosting, respectively.

shown in Figure 14. These parameters are chosen to be realistic to swell waves during acquisition. Ideally, we would do FD modelling with a ‘wavy’ curved upper surface as shown in Figure 14. However, it is difficult, in practice, to do FD modelling with a curved surface to create a ghost model that changes as a function of offset. Instead, we approximate the variability in the ghost model by changing the vertical receiver ghost positions as shown in Figure 14. We follow a similar workflow to create synthesized data from the section ‘Methodology – Kirchhoff demigration’. However, the vertical positions of receivers above the still-water line change as a function of offset and also change for each shot, as shown in Figures 14 and 15. The swell wave changes for each shot by using a phase shift from Equation (3) that depends on the shot increment and relative wave speed. We assume that the source ghost does not change during this test and acquisition in general. The air-gun array is often positioned close to the sea surface and follows the vertical motion of the waves. This scenario generates a receiver ghost that changes with offset and from shot to shot, as shown in Figure 15c,d. The swell wave moves slowly compared to the seismic waves so we can assume that the sea surface does not change within

a shot record. We assume furthermore that the tilt of the sea surface is negligible because of the small ratio between the wave height and wavelength. Modelling a ghost this way is a simplification of a real marine environment. A more realistic dynamic sea surface could be modelled using the approach by Blacquière and Sertlek (2019). However, this test should be realistic enough to help understand how sensitive the network is to changes in the ghost model. The effect of these swell waves on the receiver ghost is visible on a shot gather and a common channel gather shown in Figure 15. We first test the network trained on a constant streamer depth of 20 m (from the ‘Baseline test’ subsection) and the conventional deghosting method by Poole (2013) using parameters consistent with a constant streamer depth of 20 m. The NRMS error using the DEGDDEM (U-net) deghosting, DEGDDEM (DU-net) deghosting and conventional deghosting is 0.0044, 0.0064, and 0.0171, respectively. Figure 16 shows the DEGDDEM (U-net) and conventional deghosting results and errors using both methods. Both DEGDDEM and the conventional deghosting leave residual ghost that appears as a ‘grainy’ pattern in Figure 16, because of the cyclical period of the swells. To make DEGDDEM more robust to errors in streamer

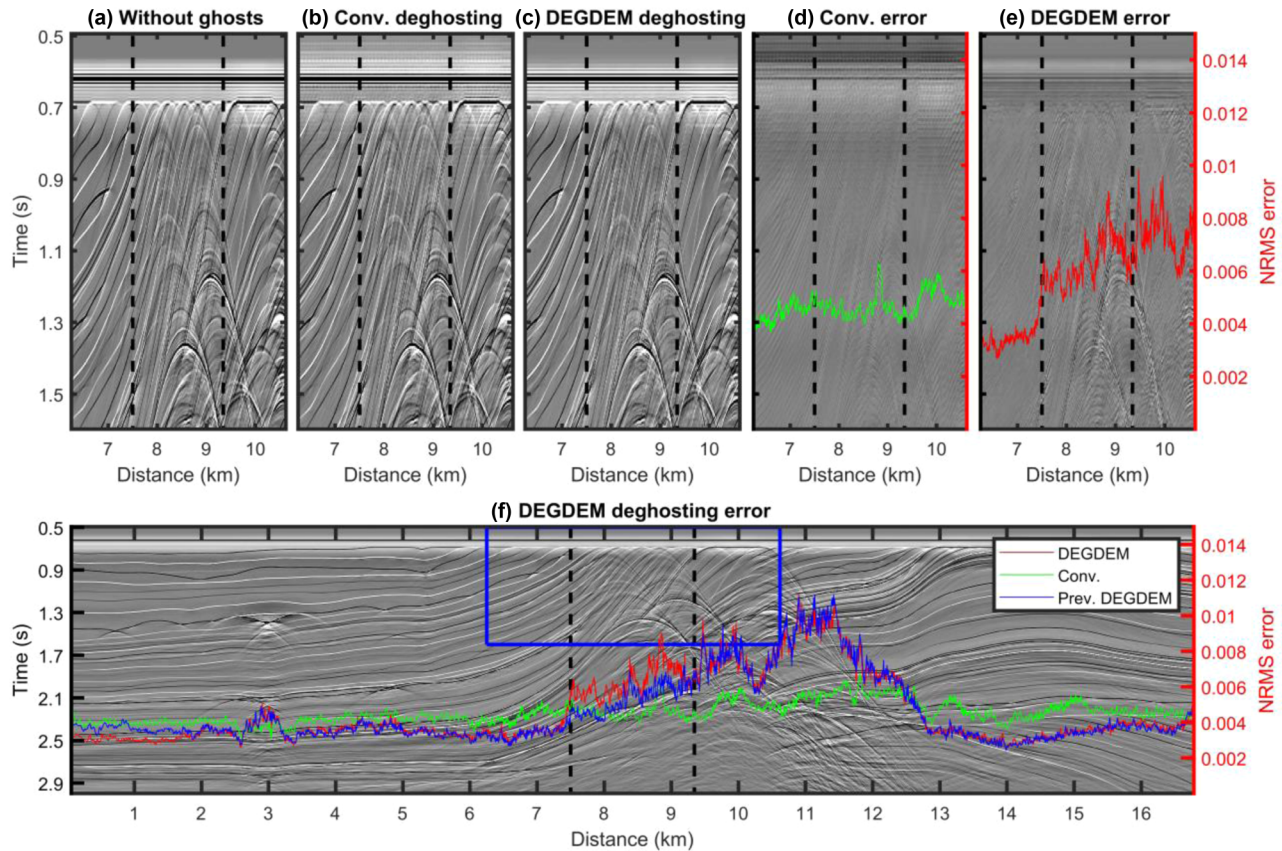


FIGURE 13 Common channel gathers (receiver 15) before deghosting (a), conventional deghosting (b), DEGDEM deghosting (c), the conventional deghosting error (d), the DEGDEM deghosting error (e) and a zoom out of the DEGDEM deghosting (f). The area shown in subfigures a, b, c, d and e is indicated by a blue rectangle in subfigure f. The area between the dashed lines is not used as training data. The red, green and blue lines show the NRMS error using DEGDEM, conventional deghosting and the previous DEGDEM network (shown in Figure 12), respectively.

depth, we trained a U-net and a DUnet on flat streamers with depths ranging from 18 to 22 m with a 0.5-m increment. The NRMS error using the U-net and DUnet are 0.0039 and 0.0078, respectively. The U-net shows an improvement from training only on one streamer depth. However, the DUnet showed a worse result, which indicated that this structure might not be ideal when making a robust network to swell waves. There are endless opportunities to create training data with streamer depth perturbations. In this example, we show the simplest perturbation. However, a constant streamer depth perturbation is sufficient to make the U-net more robust to changes in streamer depth due to swells. The results also show that both networks are less sensitive to changes in streamer depth compared to conventional deghosting. Note that it is possible to incorporate a variable sea surface datum in conventional deghosting (see, e.g., King & Poole, 2015). However, this could complicate the workflow as it requires the computation of wave heights prior to the deghosting.

Second, a simple test was done to test the sensitivity and generalization of the sea surface reflection coefficient. The real reflection coefficient will change with incidence angle

and frequency and is dependent on the sea state (Orji et al., 2013; Asgedom et al., 2017), which makes it complicated to estimate. We simplify by assuming that the reflection coefficient is constant. We generate FD data with a reflection coefficient of -0.92 for both the source and receiver ghosts. We test the baseline networks that are trained on data with a reflection coefficient of -1 from the subsection ‘Baseline test’. We compare these networks with the conventional deghosting method by Poole (2013) using parameters consistent with a reflection coefficient of -1 . The NRMS error using DEGDEM (U-net), DEGDEM (DUnet) and conventional deghosting is 0.0039, 0.0050, and 0.0058, respectively. Moreover, a generalized U-net and DUnet were trained on reflection coefficients ranging from -0.90 to -1 with an increment of 0.02. The NRMS error using the U-net and DUnet was 0.0031 and 0.0028, respectively. These results indicate that the networks were less sensitive than the conventional method to the change in sea surface reflection coefficient. In addition, the result also showed a significant improvement if the networks were generalized.

Water velocity can also change during the acquisition and deviate from the estimated water velocity, consequently

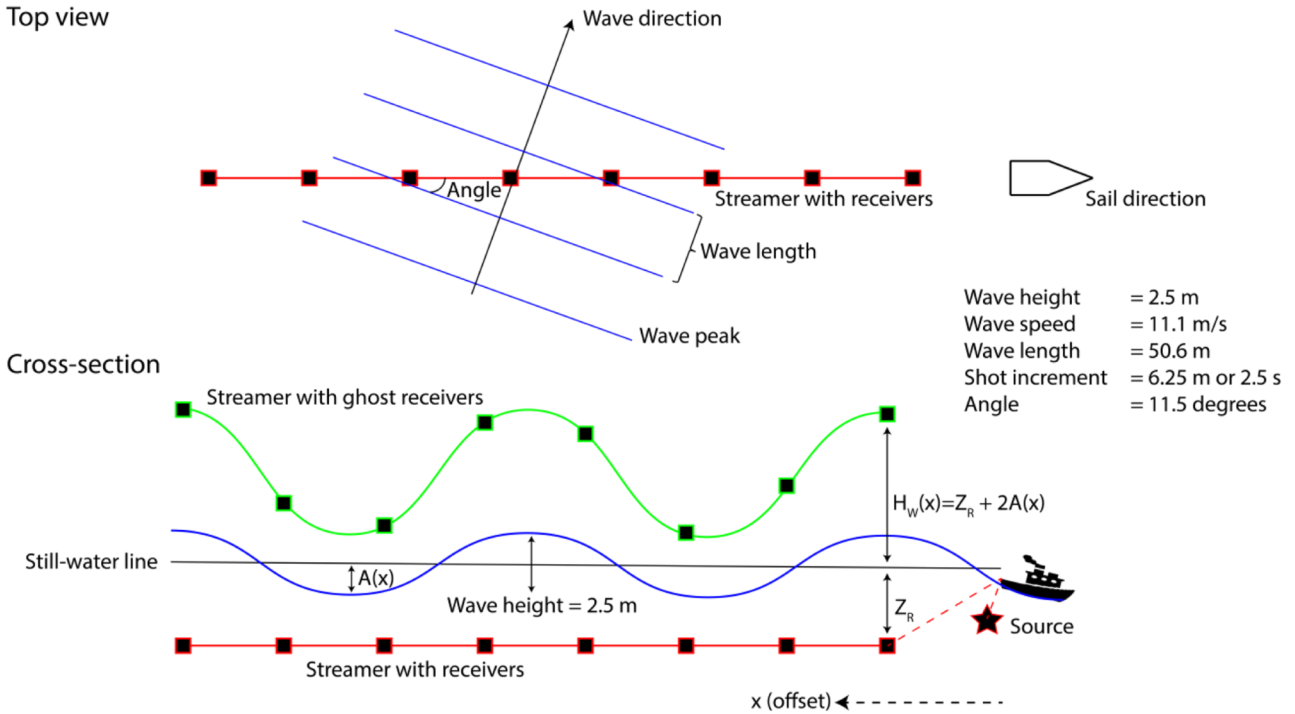


FIGURE 14 Illustration showing how receiver depth changes with offset and between shots because of swell waves. It also demonstrates how we create the receiver ghost by changing the ghost receiver height (H_W) above the still-water line.

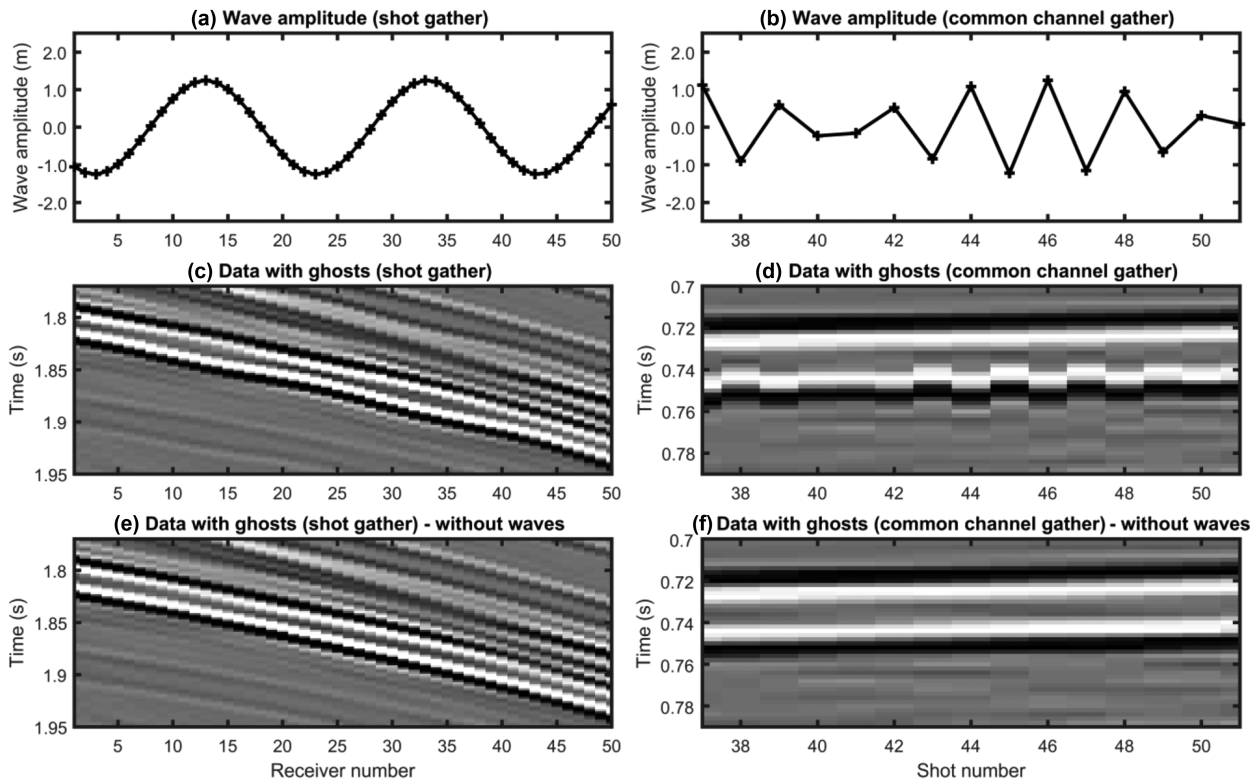


FIGURE 15 (a) The swell wave amplitude above the still-water line as a function of receiver number. (b) The swell wave amplitude above the still-water line as a function of shot number. (c) Shot gather with source and receiver ghosts. (d) Common channel gather with source and receiver ghosts. (e) and (f) show how the data would look like without the swell wave in a shot gather and a common channel gather, respectively. The top black and white events are the primary and source ghost, respectively. The following white and black events are the receiver and source–receiver ghosts, respectively.

changing the time lag of the ghosts. However, it is likely that a generalized DEGDEM would be able to account for these changes equally well as changes in timing caused by other factors (such as swells).

Sensitivity to residual ghost in the reflectivity model

One potential limitation of the workflow shown in Figure 2 is the presence of a residual ghost in the data before migration. The residual ghost is caused by imperfect deghosting and will be included in the PSDM image after migration and, consequently, the synthesized demigrated training data. To investigate this, we apply a deliberately imperfect deghosting on the synthetic data, which will lead to residual ghosts in the PSDM image. The first part of the workflow shown in Figure 7 is changed to the workflow shown in Figure 17.

We use synthetic data with swell waves from the previous subsection ‘Sensitivity and generalization to streamer depth and sea surface reflection coefficient’. We deghosted the data using conventional deghosting assuming 20 m streamer depth, which led to imperfect deghosting and residual ghosts as shown in Figure 16c. This deghosted data ended up in the PSDM image, and we created synthesized data using Kirchhoff demigration with a 20-m streamer depth. These data were used to train the U-net and DUNet that were applied to data with swell waves. The result using the DEGDEM (U-net) deghosting and DEGDEM (DUNet) deghosting gave an NRMS error of 0.0070 and 0.0081, respectively. The error using conventional deghosting and DEGDEM (U-net) are shown in Figure 18. As shown in the previous subsection, the NRMS error using conventional deghosting and a U-net trained on data from a clean reflectivity model (but 20 m constant streamer depth) were 0.0171 and 0.0044 (Figure 16), respectively. These results show an improvement from the conventional method. However, these results also show that the networks are sensitive to residual ghost in the PSDM image.

Surface-related multiples in the test data

Up to this point, we have shown examples of primary reflections (which correspond to only one reflection from each reflector or diffractor in the subsurface) containing ghosts. However, real data also contains multiple reflections (which experience more than one reflection from the subsurface) which also have ghosts. One potential limitation of the

DEGDEM workflow (Figure 2) is that Kirchhoff demigration does not consider all waves which have ghosts, such as converted waves or multiples. Surface and internal multiples are problematic because they interfere with primary reflections. As a result, suppression of multiples is an essential prerequisite for accurate seismic imaging and interpretation. We will test how the network reacts when exposed to multiples in the synthetic FD data. One option to model all surface-related multiples is to use a free surface boundary condition in the FD modelling. However, with this option, we cannot generate data with multiples and without ghosts, which we need for our ground truth. In addition, if we use a free surface boundary condition, we cannot remove the multiples after deghosting to identify any primary damage caused by the deghosting. Therefore, we avoid a free surface boundary condition and generate the first-order surface-related multiples by first placing the source 900 m (twice the water depth of 450 m) above its original position and create synthetic FD data. Similarly, we place the receivers 900 m above their original position and create synthetic FD data. These two datasets are combined and multiplied by the sea surface reflection coefficient (-1) and the zero-offset reflection coefficient at the water bottom to create a close approximation to first-order multiples. Most of the multiple energy is caused by the first-order multiple. The difference is small between our multiple models and the multiples we get using a free surface boundary condition in the FD modelling. The data with and without multiples included are shown in Figure 19a,b with blue arrows highlighting surface-related multiples. We use the same networks as in the subsection ‘Baseline test’ and apply them to this data with surface-related multiples. Figure 19 shows the results using DEGDEM (U-net) and conventional deghosting. After deghosting, we remove the surface-related multiples to investigate if there is any primary damage or imperfect deghosting caused by the multiples (Figure 19e,f). Visually, we observe the source, receiver and source–receiver ghosts removed from the data using either DEGDEM or conventional deghosting. In addition, the primaries seem to be preserved at locations where primary and multiple overlaps. However, the blue arrow at 2 s in Figure 19g,h shows some error in deghosting. The NRMS error using DEGDEM (U-net), DEGDEM (DUNet) and conventional deghosting before demultiple is 0.0042, 0.0040 and 0.0040, respectively. As in the baseline test, the conventional deghost worked better than DEGDEM at the ghost peak frequencies, and DEGDEM performed better at the ghost notches. This simple test demonstrates that the networks can remove ghosts of multiples. A combination of source- and receiver-side multiples along with other multiple generators would complicate this analysis.

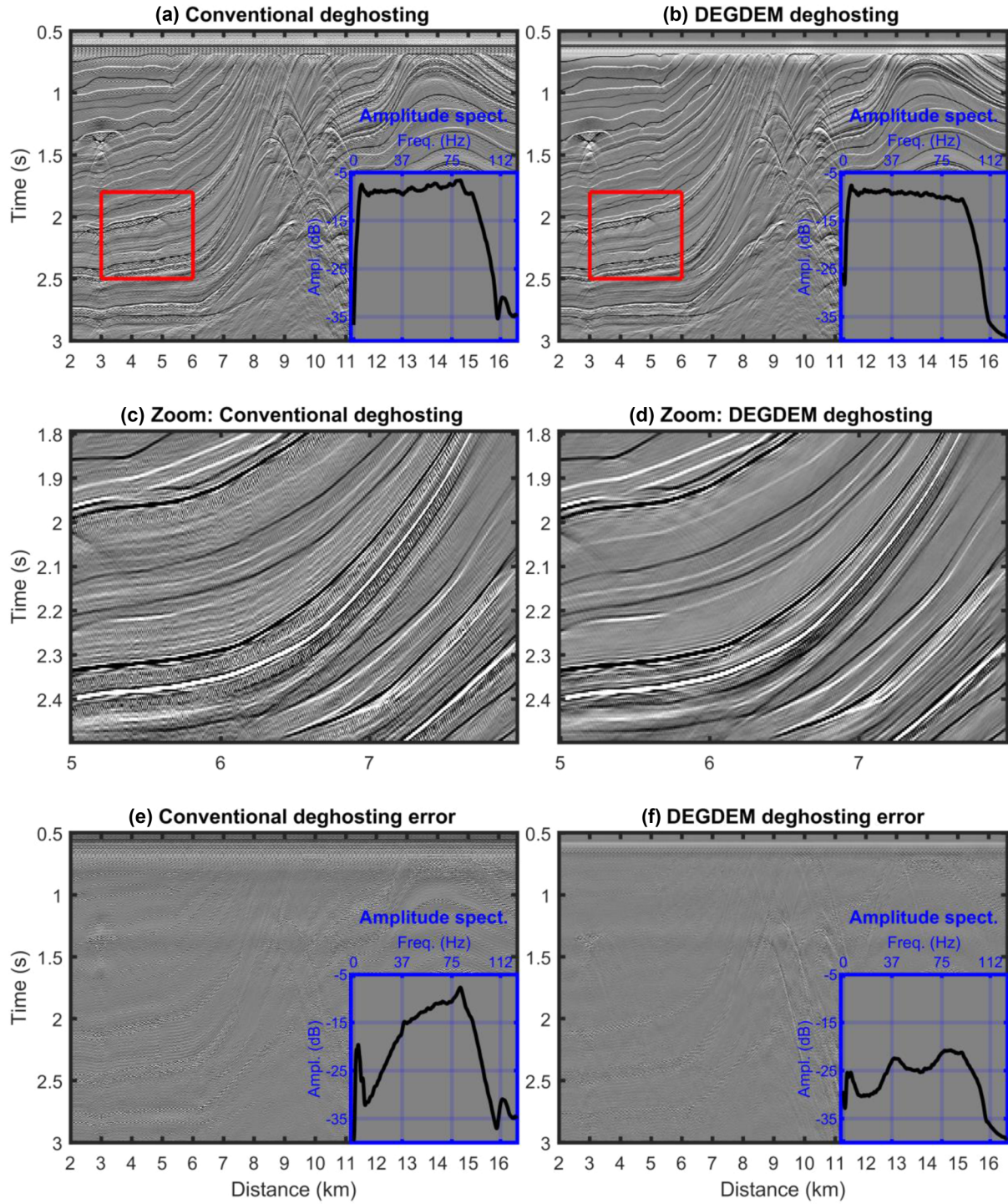


FIGURE 16 (a) Conventional deghosting, (b) DEGDEM deghosting, (c) Conventional deghosting zoom (shown as a red rectangle in subfigure a), (d) DEGDEM deghosting zoom, (e) conventional deghosting error (NRMS = 0.0171) and (f) DEGDEM deghosting error (NRMS = 0.0044).

Real data: PL988 Tampen

The real data used in this paper are from a survey located in the North Sea, Tampen area (PL988) off the western coast of Norway. CGG acquired these data in 2015 and 2016. The survey used a variable streamer depth configuration

(Soubaras & Dowle, 2010; Soubaras et al., 2012) with dual-level source arrays (Siliqi et al., 2013) as shown in Figure 20. In total, the survey has 12 streamers and two sources. We have data before deghosting, a PSDM image and a smooth velocity model. Using the survey geometry for all cables and both sources, we generated a trained CNN model using DEGDEM

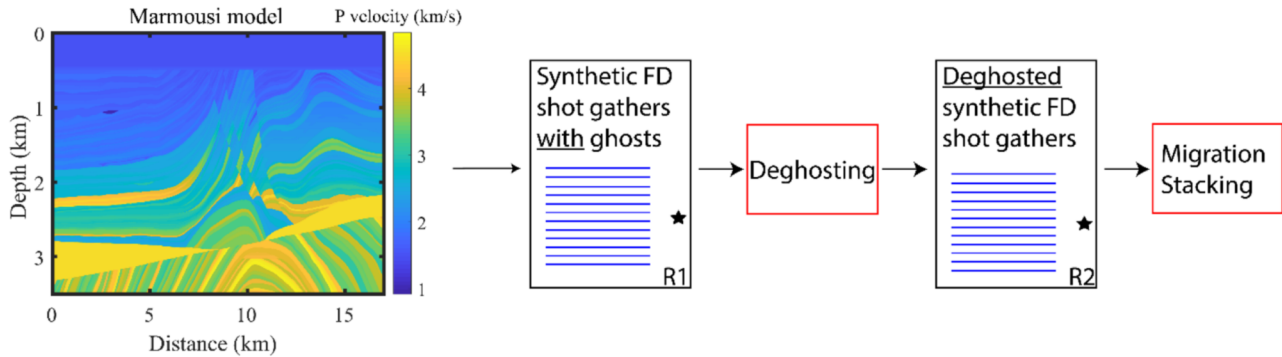


FIGURE 17 Workflow used to test the sensitivity to residual ghost in the PSDM image.

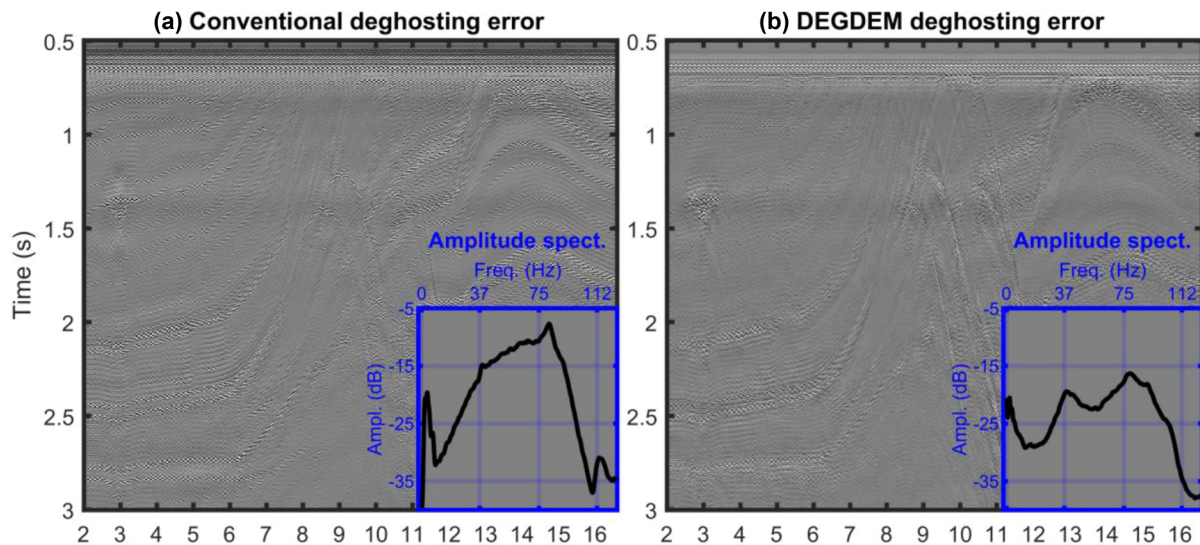


FIGURE 18 (a) Conventional deghosting error (NRMS = 0.0171) and (b) DEGDEM deghosting error (NRMS = 0.0070).

and applied the network on the real data before deghosting and compared it with conventional deghosting (Poole, 2013). We assumed a single level source at 6 m for conventional deghosting and DEGDEM for simplicity purposes. Due to this assumption, both deghosting results will be suboptimal. The Discussion section will highlight that the resolution of some of these features is significantly improved by using conventional deghosting with a dual-level source.

We show our results in common channel gathers. This domain was chosen because we have variable streamer depth data and in this domain, we can clearly observe the ghost notches in the amplitude spectrum. In addition, the time delay from the primary to the ghosts is approximately the same. We show our results in channel 15 and channel 50 for source 1 and streamer 6 (Figure 20). The offset, depth and notch frequency for channel 15 are approximately 324 m, 10.5 m and 71 Hz, respectively. For channel 50, the offset, depth and notch frequency are approximately 762 m, 18.3 m and 41 Hz, respectively. We show only results using the U-net.

The DUnet was also used but showed similar results to the U-net and is consequently not shown. The results from channel 15 are shown in Figure 21. The amplitude spectrum in Figure 21g (calculated from 0.3 to 1.5 s) shows that DEGDEM deghosting has more energy around the ghost notch. The results (Figure 21c,d,e,f) show an increased resolution using DEGDEM deghosting. In Figure 21d,f, we also see an event (highlighted by the top-left blue arrow) that has almost disappeared using conventional deghosting but remains visible using DEGDEM deghosting. The blue arrows, in Figure 21d,f, show examples with better-defined reflectors using DEGDEM deghosting. The results from channel 50 are shown in Figure 22. The amplitude spectrum in Figure 22g (calculated from 0.92 to 1.24 s) shows that the DEGDEM deghosting has more energy around the ghost notches. A similar observation was made during the inspection of the synthetic data. Analysis of potential residual ghost energy is challenging in shallow water areas where multiple reverberations cross-cut other arrivals. It will certainly be the

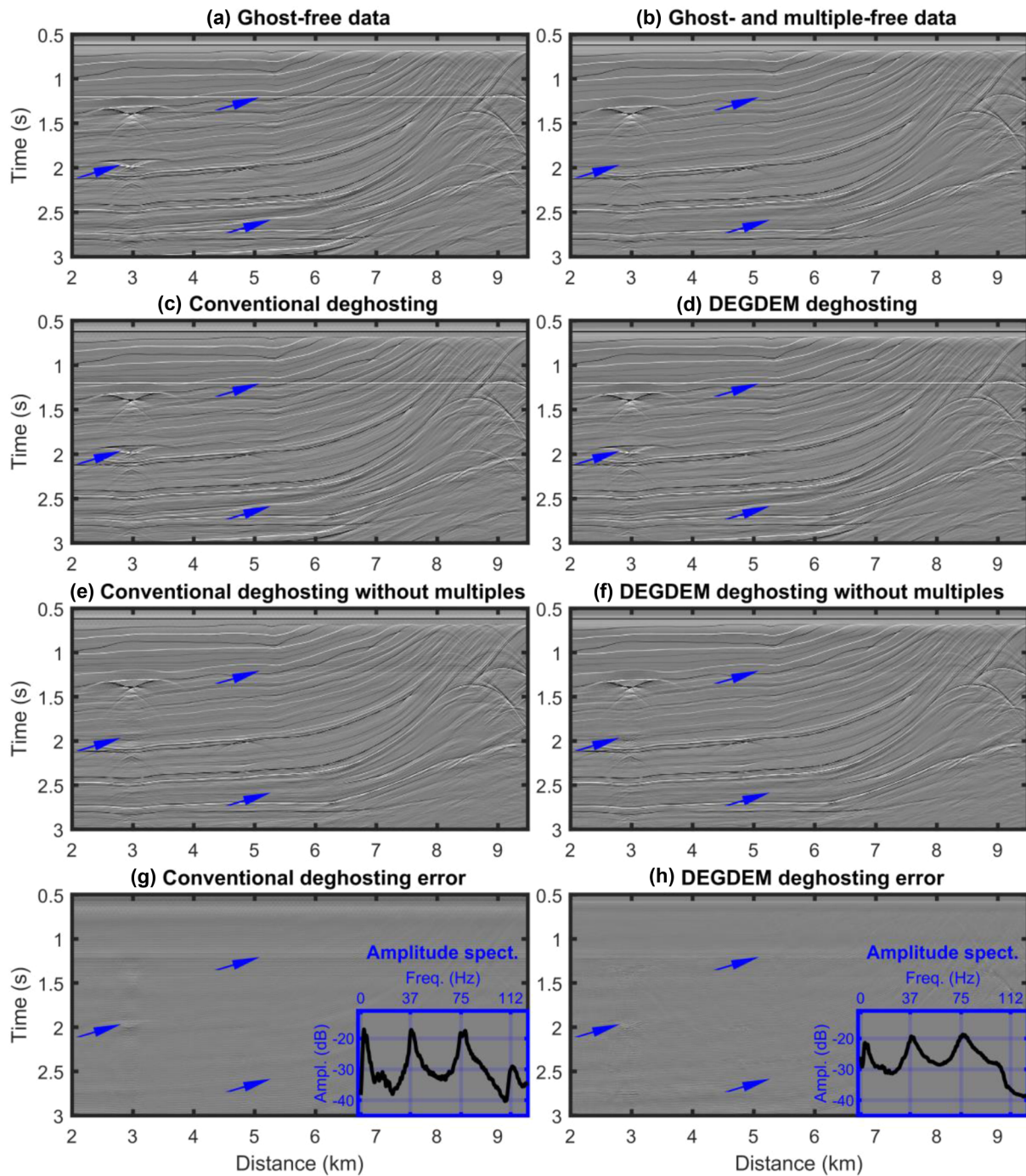


FIGURE 19 Common channel gathers without ghost and with multiples (a), without ghosts and without multiples (b), conventional deghosting (c), DEGDEM deghosting (d), conventional deghosting with multiples removed (e), DEGDEM deghosting with multiples removed (f), conventional deghosting error (g), and DEGDEM deghosting error (h). Deghosting is done before removing the multiples.

case that in some areas ghost arrivals will coincide with primary or multiple arrivals from other reflectors. The green arrows, in Figure 22a,b, highlight two arrivals with similar timing to anticipated receiver ghost energy. Figure 22c,d,e,f shows some arrivals with similar timing after deghosting. This energy is slightly weaker on the DEGDEM deghosting compared to the conventional deghosting. Figure 23 shows the

results of a shot gather. This domain illustrates that DEGDEM has removed some linear noise and weak diffraction energy. As a result, DEGDEM deghosting appears less noisy. However, given the data used in the DEGDEM training was after migration and demigration, which is known to contain inherently clean data, this result is not surprising. This linear noise is dipping in the opposite direction of the primary and is quite

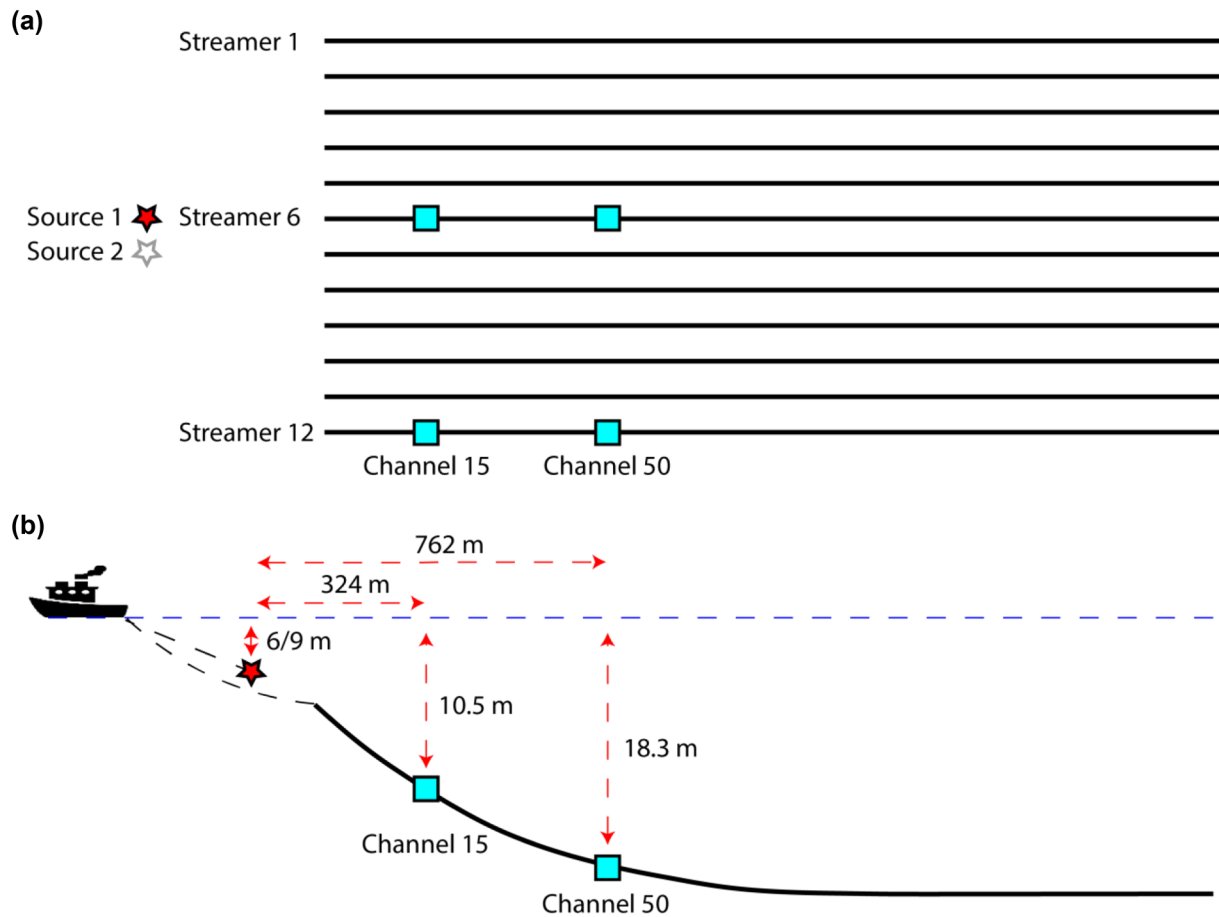


FIGURE 20 (a) Top view of the survey geometry and (b) cross section of streamer 6. Channel 15 and channel 50 are highlighted since we look at results from these channel gathers.

different from the training data. As a result, the network might not know how to handle or deghost this noise.

DISCUSSION

Synthetic data

The synthetic tests followed the same workflow as we would use on real data (excluding some processing steps such as deblending and designature because we modelled ‘clean’ finite-difference (FD) data without these types of noise). FD modelling was used to create the pre-stack depth migration (PSDM) image. Afterwards, we modelled training data with Kirchhoff demigration using the PSDM image. The network was then applied to the FD data. This approach avoided creating training data and prediction data using the same modelling approach, which could bias the results.

The ‘baseline test’ demonstrated that the neural network removed most of the ghosts and recovered amplitude in the notches (Figure 11). In addition, it also showed that the network can be trained on one part of the data and applied

successfully to another. The conventional deghosting worked better than DEGDEM (DEGHOSTING using DEMigration-based supervised learning) when source/receiver depth and sea surface reflectivity coefficient are perfectly known. DEGDEM may have performed better than conventional deghosting in the ghost notches because the training data were similar to the prediction data, which is one of the advantages when using demigration to create training data. In other words, it was already familiar with the ‘spiky’ nature of the prediction input. The conventional deghosting, on the other hand, was more general and did not have a bias towards any wavelet or geology. In addition, DEGDEM performed less well than the conventional deghosting on conflicting dipping events. This is believed to be because these conflicting dips were less well represented in the training data of the convolutional neural network (CNN). It could also be related to inaccurate demigration in the complicated areas because the migration result that leads to the PSDM image is poor in those areas. The demigration affects the training data in terms of similarity between the training data and prediction data. Another reason could be related to DEGDEM using the shot gather domain which might not be ideal for source deghosting.

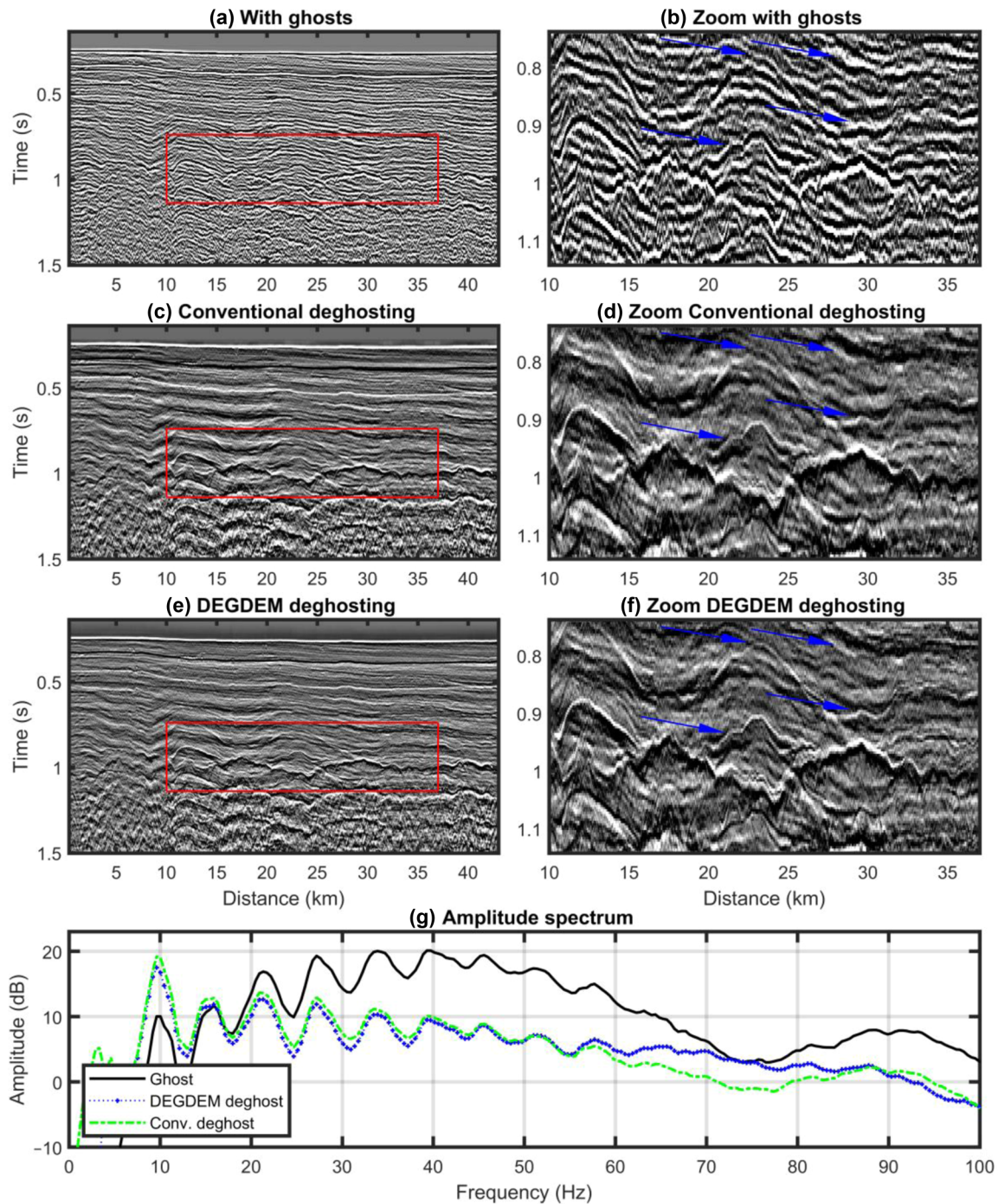


FIGURE 21 Results on real data shown in the common channel gather (channel 15). (a) and (b) Data with ghosts. (c) and (d) Conventional deghosting. (e) and (f) DEGDEM deghosting. The red area in subfigures a, c and e is used as a close-up in subfigures b, d, and f. (g) Amplitude spectrum for data with ghosts (black), DEGDEM deghosting (blue) and conventional deghosting (green). The blue arrows indicate places where the resolution is increased.

Conventional source deghosting is often carried out on receiver gathers since the source ghost notch will be a function of apparent slowness in this domain, e.g., visible in the f - k domain. However, the source ghost notch may be incorrect in the shot gather since the relation between the emission and incidence angles is not straightforward in a complex medium

(Blacqui re & Sertlek, 2019). As a result, energy with one emission angle may arrive with another or multiple angles. Correspondingly, the receiver ghost notch is better defined in the shot gathers. Consequently, receiver deghosting is often done in shot gathers. Instead of doing both the source and receiver deghosting in one operation on shot gathers, we

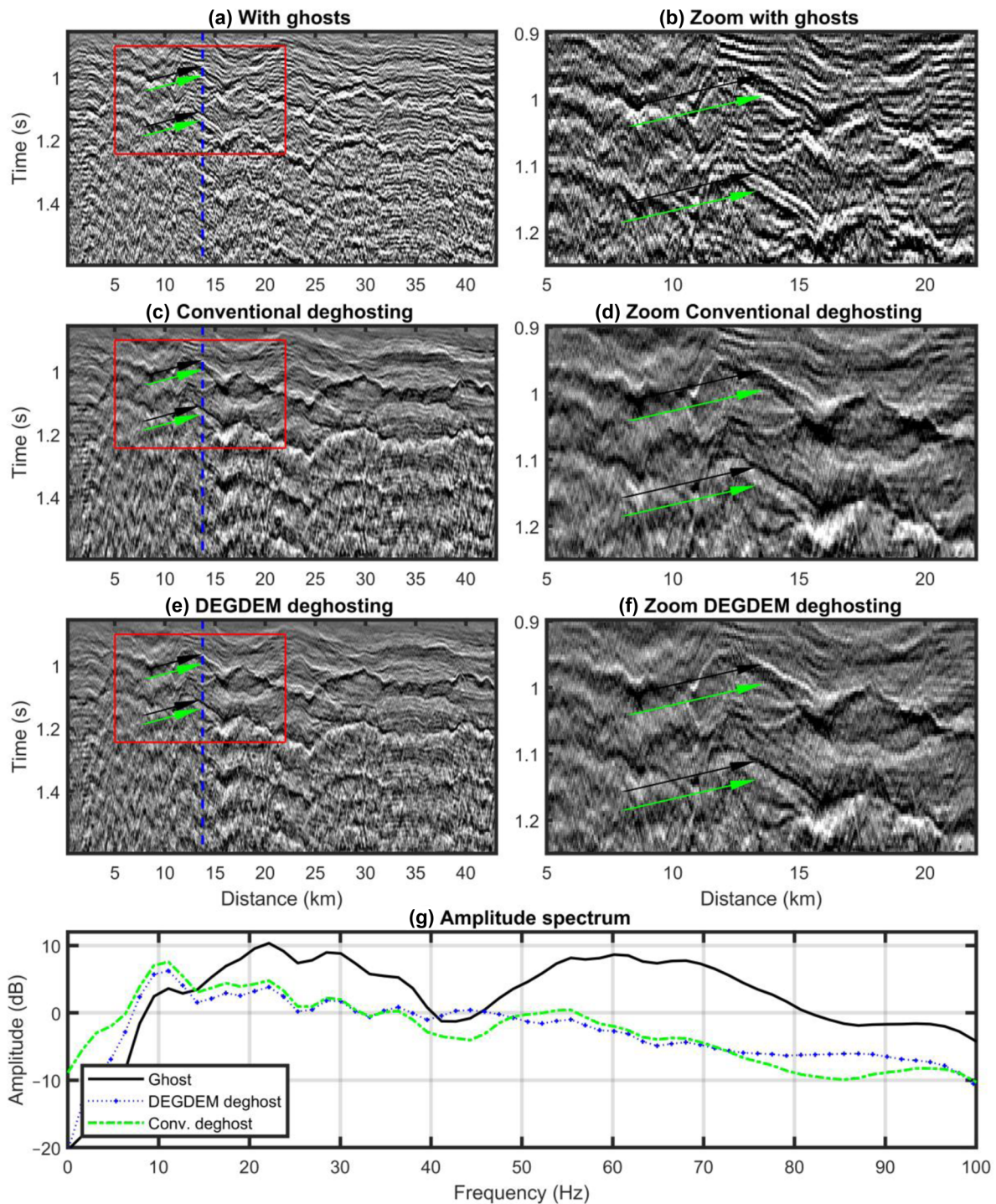


FIGURE 22 Results on real data shown in the common channel gather (channel 50). (a) and (b) Data with ghosts. (c) and (d) Conventional deghosting. (e) and (f) DEGDEM deghosting. The red area in subfigures a, c, and e is used as a close-up in subfigures b, d, and f. (g) Amplitude spectrum for data with ghosts (black), DEGDEM deghosting (blue) and conventional deghosting (green). Black arrows indicate the primary or multiple, and green arrows indicate places with receiver ghosts. The vertical dashed blue line is the location of the shots shown in Figure 23.

could create a CNN for source deghosting on receiver gathers and another CNN for receiver deghosting on shot gathers. However, this is a topic for future research.

A clear conclusion of the synthetic tests is that DEGDEM was less sensitive to swells, variations in sea surface

reflection coefficient and errors in shot/receiver depths than the conventional method. An example was demonstrated on the data without and with swells where we observed a moderate change in the normalized root mean square (NRMS) error (0.0032–0.0044) using DEGDEM (U-net) compared to

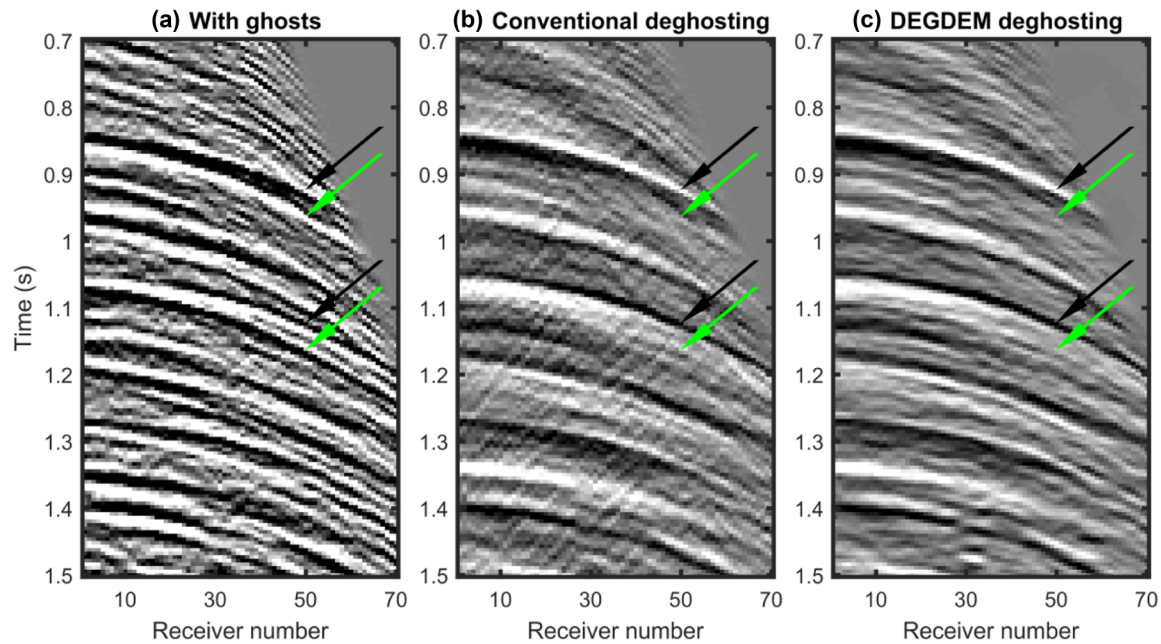


FIGURE 23 Results on real data on a shot gather. (a) Data with ghosts. (b) Conventional deghosting. (c) DEGDEM deghosting. Black arrows indicate the primary or multiple and green arrows indicate the timing of the receiver ghost. The shot location is shown in Figure 22 as a vertical dashed blue line.

the significant change in NRMS error (0.0030–0.0171) of the conventional method. It is possible to estimate the sea state (Orji et al., 2012) and use it to improve the deghosting (King & Poole, 2015; Vrolijk & Blacquièrre, 2018), but this adds more complexity to the deghosting process. Our results showed that the U-net can be made more robust to errors in streamer depths and sea surface reflection coefficients. This is potentially advantageous since there will always be some error when estimating these parameters on real data.

The test to investigate the sensitivity to residual ghost in the PSDM image showed, not surprisingly, that the networks performed less well than in the case where a fully ghost-free PSDM image was used. The DEGDEM (U-net) NRMS error using a clean PSDM image was 0.0044 versus 0.0070 when using a residual ghost PSDM image. However, the NRMS error was 0.0171 using the conventional deghosted data that went into the PSDM image. This suggests that DEGDEM can still improve on the quality of deghosting exhibited in the supplied PSDM image.

The final test demonstrated that the networks can deghost data with surface-related multiples (Figure 19) and preserve primaries interfering with multiples. This result is important since surface-related multiples are present in real data.

Real data

Our results show that the network was able to deghost real three-dimensional (3D) data. Comparing our results with the

conventional method by Poole (2013) shows that the network resulted in higher amplitudes at the ghost notches. Figure 24 shows both conventional deghosting and DEGDEM at the second ghost peak (60 ± 2 Hz) and first ghost notch (42 ± 2 Hz). Both conventional and DEGDEM give similar results in the ghost peak (Figure 24c,d). Figure 24e,f does not clearly show that DEGDEM is able to recover a more coherent signal in this ghost notch. It is not easy to assess DEGDEM's ability to 'fill' the notch on real data. In addition, it is hard to assess the level of residual ghost energy in shallow water data due to the overlap of primary and reverberating multiple arrivals. We highlight an example of a possible residual ghost arrival, which was slightly weaker in the DEGDEM result compared to the conventional deghosting result.

In the real data example, we assumed a single-level source for both DEGDEM and conventional deghosting. Dual-level source deghosting was beyond the scope of our analysis mainly due to the added complexities it introduces for the demigration stage of the DEGDEM workflow. Nevertheless, Figure 25 shares some insight into what uplift may be provided by this approach. Figure 25 (left) shows results from joint source and receiver deghosting results assuming a single-level source as described in the previous section, and Figure 25 (right) shows results from joint source and receiver deghosting assuming a dual-level source (Poole et al., 2015). The image respecting the dual-level source setup looks sharper compared to the single-level source approach. It is possible that both the conventional and DEGDEM

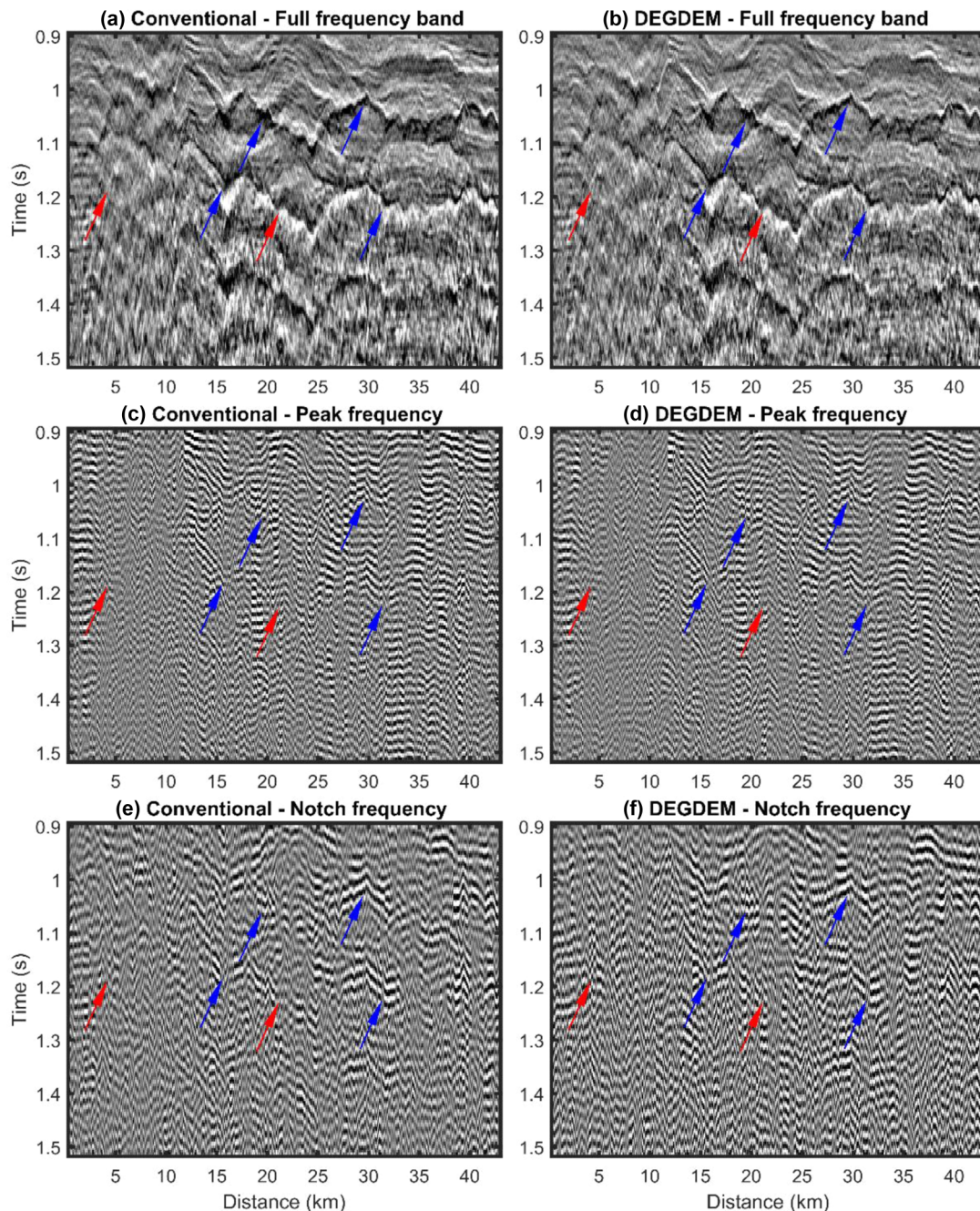


FIGURE 24 (a) Conventional deghosting using the full spectrum, (b) DEGDEM deghosting using the full spectrum, (c) conventional deghosting at the peak frequency, (d) DEGDEM deghosting at the peak frequency, (E) conventional deghosting at the notch frequency and (F) DEGDEM deghosting at the notch frequency. Blue arrows indicate a coherent signal. Red arrows indicate what we interpret as noise or lack of coherent signal

deghosting could have given a better result if we had used a dual-level source.

Our results demonstrate that a network can be used on real data with good results. The main limitation of DEGDEM is the dependency on a PSDM image. This is similar to the ‘chicken-and-egg’ problem where we need to do deghosting to get a PSDM image but need the PSDM image to do deghosting. However, there are many such problems in seismic

processing. One example is the dependency on a PSDM image to create multiple models for demultiple, but demultiple data are needed to make the PSDM image (Brittan et al., 2011; Martin et al., 2011). Another example is the dependency on a velocity model for PSDM, but PSDM is needed to make a velocity model (Chang et al., 1996). A PSDM image is not always available, for example, in a new acquisition area or the early phase of a processing project. However, a PSDM image

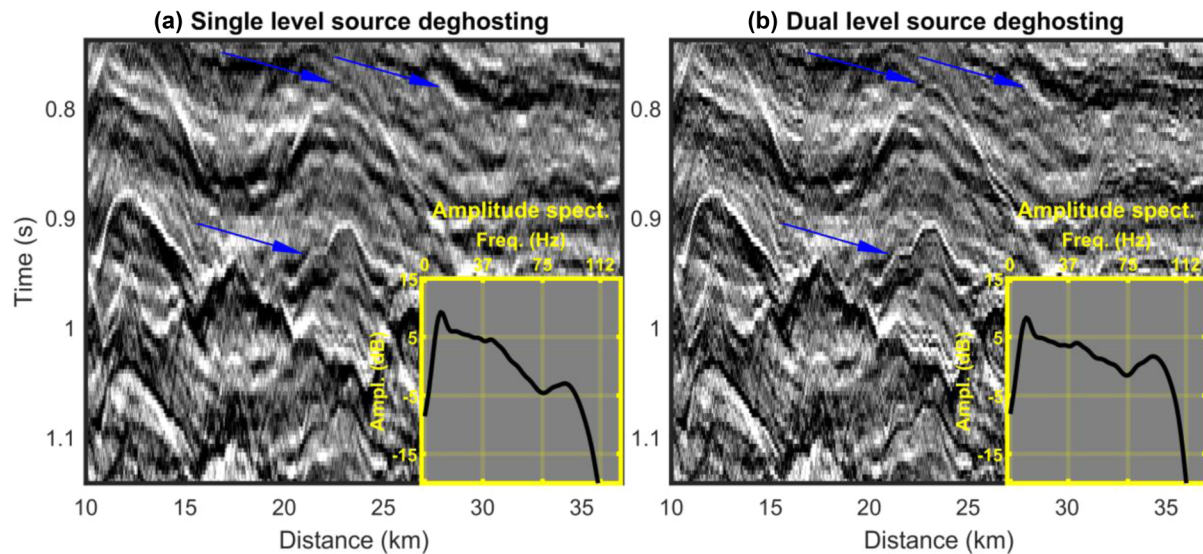


FIGURE 25 Conventional deghosting when we assume a single-level source (a) or a dual-level source (b). Blue arrows indicate better-defined reflectors

could be available from another acquisition in the same area or, as demonstrated here, from the same acquisition. Inaccuracy of migration velocity and limitation of PSDM could affect the performance of DEGDEM. It should also be noted that DEGDEM is computationally expensive since we need to create the demigrated training data, train a CNN, apply the CNN to the data and include an extra migration of the data. Assuming we already have a PSDM image, DEGDEM (U-net) is approximately 40 times slower when training and predicting on the same area compared to the conventional method used in this paper. For DEGDEM, this time includes demigration, training and prediction. The computation time for conventional deghosting and DEGDEM is highly dependent on the parameters and amount of training data used. However, it is possible that a network could be trained only on a representative part of the data and applied to the rest, similar to the method of de Jonge et al. (2021). Using that approach could eventually make DEGDEM faster than the conventional deghosting (assuming a PSDM image is already available). In principle, the basic idea behind the training approach in DEGDEM could be used for purposes other than deghosting, such as interpolation, demultiple, debubble, designature and more. However, investigating a similar workflow for these problems is a topic for future research.

CONCLUSION

The results in this paper have demonstrated that DEGDEM (DEGhosting using DEMigration-based supervised learning) is capable of removing the source and receiver ghosts on both

synthetic and real data. On synthetic tests, we observe that the network was significantly less sensitive to errors in streamer depth and sea surface reflection coefficient compared to conventional deghosting.

On real data, DEGDEM showed a good level of energy in the ghost notch and provided locally better resolution compared to conventional deghosting. We examined a potential residual ghost arrival, which looked weaker on the DEGDEM result, but as discussed, it is hard to assess the level of residual ghost in shallow water datasets as many arrivals overlap. We demonstrated the robustness of DEGDEM to unknown changes in sea-state, receiver position and sea surface reflectivity, which are unavoidable on real data.


ACKNOWLEDGEMENTS

The authors would like to thank CGG and the University of Bergen for providing the working environment for this research. We are grateful to CGG Multi-Client and Lundin for providing show rights. Further thanks go to Simon King, Karl Magnus Nielsen and the CGG internal reviewers, James Cooper and Ziqin Yu, for their helpful comments and suggestions that improved this work. We extend our gratitude to the Research Council of Norway, the University of Bergen and CGG for funding this work through an industrial Ph.D. grant, project no. 305450.

DATA AVAILABILITY STATEMENT

The real data associated with this research are confidential and cannot be released. The Marmousi model can be found online: https://wiki.seg.org/wiki/AGL_Elastic_Marmousi.

ORCID

Thomas de Jonge  <https://orcid.org/0000-0001-7834-9526>

REFERENCES

- Almuteri, K. & Sava, P. (2021) A convolutional neural network approach for ghost removal seismic deghosting using CNNs. In: *First International Meeting for Applied Geoscience & Energy Expanded Abstracts*, Society of Exploration Geophysicists, pp. 2550–2554.
- Amundsen, L. & Zhou, H. (2013) Low-frequency seismic deghosting. *Geophysics*, 78, WA15–WA20.
- Amundsen, L., Weglein, A.B. & Reitan, A. (2013a) On seismic deghosting using integral representation for the wave equation: Use of Green's functions with Neumann or Dirichlet boundary conditions. *Geophysics*, 78, T89–T98.
- Amundsen, L., Zhou, H., Reitan, A. & Weglein, A.B. (2013b) On seismic deghosting by spatial deconvolution. *Geophysics*, 78, 267–271.
- Asgedom, E.G., Ceccconello, E., Orji, O.C. & Söllner, W. (2017) *Rough sea surface reflection coefficient estimation and its implication on hydrophone-only pre-stack Deghosting*. In: 79th EAGE Conference and Exhibition 2017. EAGE, pp. 12–15.
- Aytun, K. (1999) The footsteps of the receiver ghost in the f-k domain. *Geophysics*, 64, 1618–1626.
- Bearth, R.E. & Moore, N.A. (1989) *Air gun-slant cable seismic results in the Gulf of Mexico*. In: 1989 SEG Annual Meeting. SEG, pp. 649–652.
- Blacquière, G. & Sertlek, H.Ö. (2019) Modeling and assessing the effects of the sea surface, from being flat to being rough and dynamic. *Geophysics*, 84, T13–T27.
- Brittan, J., Martin, T., Bekara, M. & Koch, K. (2011) 3D shallow water demultiple – extending the concept. *First Break*, 29, 97–101.
- Carlson, D., Long, A., Söllner, W., Tabti, H., Tenghamn, R. & Lunde, N. (2007) Increased resolution and penetration from a towed dual-sensor streamer. *First Break*, 25, 71–77.
- CGG. (2020) NVG 3D seismic. Available at <https://www.cgg.com/multi-client-data/multi-client-seismic/northern-viking-graben> (Accessed: 01 August 2022).
- Chang, H., Solano, M., VanDyke, J.P., McMechan, G.A. & Epli, D. (1996) 3-D prestack Kirchhoff depth migration: From prototype to production in a MPP environment. *Geophysics*, 63, 546–556.
- Cunha, A., Pochet, A., Lopes, H. & Gattass, M. (2020) Seismic fault detection in real data using transfer learning from a convolutional neural network pre-trained with synthetic seismic data. *Computers and Geosciences*, 135, 1–9.
- Dumoulin, V. & Visin, F. (2016) A guide to convolution arithmetic for deep learning [preprint]. ArXiv, 1603.07285.
- Fang, W., Fu, L., Zhang, M. & Li, Z. (2021) Seismic data interpolation based on U-net with texture loss. *Geophysics*, 86, V41–V54.
- Goodfellow, I., Bengio, Y. & Courville, A. (2016) *Deep Learning*. MIT Press.
- Greiner, T.L., Kolbjørnsen, O., Lie, J.E., Nilsen, E.H., Evensen, A.K. & Gelius, L. (2019) *Cross-streamer wavefield interpolation using deep convolutional neural network*. In: SEG Technical Program Expanded Abstracts 2019. SEG, pp. 2207–2211.
- Hill, D., Combee, C. & Bacon, J. (2006) Over/under acquisition and data processing: The next quantum leap in seismic technology? *First Break*, 24, 81–96.
- Hubral, P., Schleichert, J. & Tygel, M. (1996) A unified approach to 3-D seismic reflection imaging, Part I: Basic concepts. *Geophysics*, 61, 742–758.
- de Jonge, T., Vinje, V., Poole, G., Hou, S. & Iversen, E. (2021) De-bubbling Seismic Data using a Generalized Neural Network. *Geophysics*, 87, V1–V14.
- Jovanovich, D.B., Sumner, R.D. & Akins-Easterlin, S.L. (1983) Ghosting and marine signature deconvolution: A prerequisite for detailed seismic interpretation. *Geophysics*, 48, 1468–1485.
- King, S. & Poole, G. (2015) Hydrophone-only receiver deghosting using a variable sea surface datum. In: *SEG Technical Program Expanded Abstracts*. SEG, pp. 4610–4614.
- Klochikhina, E., Crawley, S., Frolov, S., Chemingui, N. & Martin, T. (2020) Leveraging deep learning for seismic image denoising. *First Break*, 38, 41–48.
- Li, J., Wang, B., Han, D. & Wang, Y. (2020) *Intelligent seismic deblending based deep learning based U-net*. In: 82nd EAGE Annual Conference and Exhibition, 2020. EAGE, pp. 1–5.
- Lucas, A., Iliadis, M., Molina, R. & Katsaggelos, A.K. (2018) Using deep neural networks for inverse problems in imaging: beyond analytical methods. *IEEE Signal Processing Magazine*, 35, 20–36.
- Martin, G.S., Wiley, R. & Marfurt, K.J. (2006) Marmousi2: An elastic upgrade for Marmousi. *Leading Edge (Tulsa, OK)*, 25, 156–166.
- Martin, T., Brittan, J., Bekara, M. & Koch, K. (2011) 3D shallow water demultiple - Extending the concept. In: 73rd European Association of Geoscientists and Engineers Conference and Exhibition 2011: Unconventional Resources and the Role of Technology. *Incorporating SPE EUROPEC 2011*, 3. European Association of Geoscientists and Engineers, pp. 2040–2045.
- Mellier, G. & Tellier, N. (2018) *Considerations about multi-sensor solid streamer design*. In: EAGE Marine Acquisition Workshop, Oslo, Norway. EAGE, cp-560-0000.7.
- Orji, O.C., Söllner, W. & Gelius, L.J. (2012) Effects of time-varying sea surface in marine seismic data. *Geophysics*, 77, P33–P43.
- Orji, O.C., Sollner, W. & Gelius, L.J. (2013) Sea surface reflection coefficient estimation. In: Society of Exploration Geophysicists International Exposition and 83rd Annual Meeting, SEG 2013. *Expanding Geophysical Frontiers*. SEG, pp. 51–55.
- Peng, C., Jin, H. & Wang, P. (2014) *Noise attenuation for multi-sensor streamer data via cooperative de-noising*. In: Society of Exploration Geophysicists International Exposition and 84th Annual Meeting SEG 2014. SEG, pp. 1878–1882.
- Peng, H., Messud, J., Salaun, N., Hammoud, I., Jeunesse, P., Lesieur, T. & Lacombe, C. (2021) *Proposal of the Dunet neural network architecture: deghosting example and theoretical analysis*. In: 82nd EAGE Annual Conference & Exhibition. EAGE, pp. 1–5.
- Poole, G. (2013) Pre-migration receiver de-ghosting and re-datuming for variable depth streamer data In: Society of Exploration Geophysicists International Exposition and 83rd Annual Meeting, SEG 2013. *Expanding Geophysical Frontiers*. SEG, pp. 4216–4220.
- Poole, G. & Cooper, J. (2018) *Multi-sensor receiver deghosting using data domain sparseness weights*. In: 80th EAGE Conference and Exhibition 2018: Opportunities Presented by the Energy Transition. EAGE, pp. 1–5.
- Poole, G., Cooper, J., King, S. & Wang, P. (2015) *3D source designation using source-receiver symmetry in the shot tau-px-py domain*. In: 77th EAGE Conference and Exhibition 2015: Earth Science for Energy and Environment. EAGE, pp. 3867–3871.
- Qu, S., Verschuur, E., Zhang, D. & Chen, Y. (2021) Training deep networks with only synthetic data: deep-learning-based near-offset reconstruction for (closed-loop) surface-related multiple estimations on shallow-water field data. *Geophysics*, 86, A39–A43.

- Rickett, J.E., van Manen, D.J., Loganathan, P. & Seymour, N. (2014) *Slanted-streamer data-adaptive deghosting with local plane waves*. In: *76th EAGE Conference and Exhibition 2014*. EAGE, pp. 1–5.
- Ronneberger, O., Fischer, P. & Brox, T. (2015) *U-net: convolutional networks for biomedical image segmentation*. In: *International Conference on Medical Image Computing and Computer-Assisted Intervention*. Springer, pp. 234–241.
- Santos, L. T., Schleicher, J., Tygel, M. & Hubral, P. (2000a) Seismic modeling by demigration. *Geophysics*, 65, 1281–1289.
- Santos, L. T., Schleicher, J., Tygel, M. & Hubral, P. (2000b) Modeling, migration, and demigration. *Leading Edge (Tulsa, OK)*, 19, 712–715.
- Schuster, G.T. (1993) Least-squares cross-well migration. In: *SEG Technical Program Expanded Abstracts*. SEG, pp. 110–113.
- Siahkoobi, A., Kumar, R. & Herrmann, F. (2018) *Seismic data reconstruction with generative adversarial networks*. In: *80th EAGE Conference and Exhibition 2018: Opportunities Presented by the Energy Transition, 2018*. EAGE, pp. 1–5.
- Siliqi, R., Payen, T., Sablon, R. & Desrues, K. (2013) Synchronized multi-level source, a robust broadband marine solution. In: *SEG Technical Program Expanded Abstracts 2013*. Society of Exploration Geophysicists, pp. 56–60.
- Song, J.G., Gong, Y.L. & Li, S. (2015) High-resolution frequency-domain Radon transform and variable-depth streamer data deghosting. *Applied Geophysics*, 12, 564–572.
- Soubaras, R. (2010) *Deghosting by joint deconvolution of a migration and a mirror migration*. In: *Annual Meeting SEG Denver 2010 Annual Meeting*. SEG, pp. 3406–3410.
- Soubaras, R. & Dowle, R. (2010) Variable-depth streamer - a broadband marine solution. *First Break*, 28, 89–96.
- Soubaras, R., Dowle, R. & Sablon, R. (2012) BroadSeis: Enhancing interpretation and inversion with broadband marine seismic. *CSEG Recorder*, 37, 41–46.
- Sun, J., Slang, S., Elboth, T., Greiner, T. L., McDonald, S. & [J] Gelius, L. (2019) Attenuation of marine seismic interference noise employing a customized U-Net. *Geophysical Prospecting*, 68, 845–871.
- Vrolijk, J.-W. & Blacquièrè, G. (2021) Source deghosting of coarsely sampled common-receiver data using a convolutional neural network. *Geophysics*, 86, V185–V196.
- Vrolijk, J. & Blacquièrè, G. (2018) Adaptive deghosting including the rough and time variant sea surface. In: *80th EAGE Conference and Exhibition 2018: Opportunities Presented by the Energy Transition*. EAGE, pp. 1–5.
- Vrolijk, J.W. & Blacquièrè, G. (2020) Source deghosting of coarsely sampled common-receiver data using machine learning. In: *SEG Technical Program Expanded Abstracts*. SEG, pp. 3294–3298.
- Zhang, Z., Masoomzadeh, H. & Wang, B. (2018) Evolution of deghosting process for single-sensor streamer data from 2D to 3D. *Geophysical Prospecting*, 66, 975–986.
- Zu, S., Cao, J., Qu, S. & Chen, Y. (2020) Iterative deblending for simultaneous source data using the deep neural network. *Geophysics*, 85, V131–V141.

How to cite this article: de Jonge, T., Vinje, V., Zhao, P., Poole, G. & Iversen, E. (2022) Source and receiver deghosting by demigration-based supervised learning. *Geophysical Prospecting*, 1–26. <https://doi.org/10.1111/1365-2478.13253>